

# **Transverse spin effects in SIDIS at 11 GeV with a transversely polarized target using the CLAS12 Detector**

H. Avakian<sup>1</sup>, S. Boyarinov, V.D. Burkert, A. Deur, L. Elouadrhiri, T. Kageya,  
V. Kubarovsky, M. Lowry, B. Musch, A. Prokudin, A. Sandorfi, Yu. Sharabian, S. Stepanyan, X. Wei  
Jefferson Lab, Newport News, VA 23606, USA

F. Klein<sup>1</sup>

Department of Physics, The Catholic University of America, Washington, DC 20064, USA

M. Aghasyan<sup>1</sup>, E. De Sanctis, D. Hasch, L. Hovsepyan, V. Lucherini

M. Mirazita, and S. Anefalos Pereira, S. Pisano, P. Rossi

LNF INFN, Frascati, I-00044, Rome Italy

K. Joo<sup>1</sup>, N. Markov, M. Ungaro

University of Connecticut, Storrs, CT 06269, USA

L. Barion, G. Ciullo, M. Contalbrigo<sup>1,2</sup>, P.F. Dalpiaz, P. Lenisa, L.L. Pappalardo, M. Statera

University of Ferrara and INFN Ferrara, Via Saragat, I-44100, Ferrara, Italy

G. De cataldo, R. De Leo, L. La Gamba, E. Nappi

University of Bari and INFN Bari, Via Orabona, I-70125, Bari, Italy

M. Battaglieri, A. Celentano, R. De Vita, M. Osipenko, G. Ricco, M. Ripani, M. Taiuti

Y. Prok

Christopher Newport University

K. Griffioen

College of William & Mary, 23187, USA

INFN Genova, Via Dodecaneso, 33 I-16146 Genova, Italy

V. Bellini, A. Giusa, F. Mammoliti, R. Potenza, G. Russo, L. Sperduto, C. Sutura

University of Catania and INFN Catania, Via S. Sofia, I-95123 Catania, Italy

R. Perrino

INFN Lecce, Via Arnesano, I-73100 Lecce, Italy

K. Hafidi, J. Arrington, L. El Fassi, D. F. Geesaman, R. J. Holt,

D. H. Potterveld, P. E. Reimer, P. Solvignon

Argonne National Lab, Argonne, IL 60439, USA

J. Ball, A. Fradi, M. Garçon, M. Guidal, S. Niccolai, F. Sabatié

IPNO (Orsay), SPhN (Saclay) France

---

<sup>1</sup>Co-spokesperson

<sup>2</sup>Contact person

M. Amarian, G. Dodge, G. Gavalian Old Dominion University, Norfolk, VA 23529, USA

A. D'Angelo, C. Schaerf, I. Zonta

Dipartimento di Fisica, Universita' di Roma Tor Vergata,

INFN Sezione di Roma Tor Vergata, Via della Ricerca Scientifica, I-00133, Rome, Italy

A. Biselli

Fairfield University, Fairfield CT 06824, USA

F. Meddi, G.M. Urciuoli

INFN Roma I, P.le aldo Moro, I-00185, Roma, Italy

E. Cisbani, A. Del Dotto, F. Garibaldi, S. Frullani

INFN Roma I and Istituto Superiore di Sanita', Viale Regina Elena, I-00161, Roma, Italy

M. Capogni

INFN Roma I and ENEA Casaccia, Via Anguillarese, I-00123, Roma, Italy

A. Puckett Los Alamos National Laboratory, Los Alamos, NM 87545, USA

M. Anselmino, A. Kotzinian, B. Parsamyan,

Università di Torino and INFN, Sezione di Torino, Via P. Giuria 1, I-10125 Torino

A. Bacchetta, M. Radici, B Pasquini

Università di Pavia and INFN Sezione di Pavia, via Bassi 6, 27100 Pavia, Italy

M. Anselmino, A. Kotzinian, B. Parsamyan

Università di Torino and INFN, Sezione di Torino, Via P. Giuria 1, I-10125 Torino

L. Gamberg

Penn State Berks, Reading, PA 19610, USA

## Abstract

We propose to study spin azimuthal asymmetries in semi-inclusive DIS (SIDIS) using an 11 GeV polarized electron beam from the upgraded CEBAF facility and the CLAS12 detector equipped with a transversely polarized target. The main focus of the experiment will be the measurement of transverse target single- and double-spin asymmetries (TTSA) in the reaction  $ep^\uparrow \rightarrow ehX$ , where  $h$  is a meson (e.g. a pion or a kaon) and  $X$  is the undetected final state. In particular, three single-spin asymmetries (SSA) will be measured, each providing access to a specific leading-twist parton distribution function (PDF): the transversity, the Sivers function and the so-called “pretzelosity” function. In a transversely polarized nucleon, the Sivers function describes the distribution of unpolarized quarks, whereas the transversity and “pretzelosity” functions describe the distribution of transversely polarized quarks. The transversity is the least known of the three fundamental collinear PDFs of the nucleon, while the Sivers and the “pretzelosity” functions are transverse-momentum-dependent (TMD) PDFs, i.e. they vanish in the collinear approximation. The joint use of a longitudinally polarized beam and a transversely polarized target will also allow us to measure double-spin asymmetries (DSA) related to an unmeasured leading-twist TMD distribution function describing the distribution of longitudinally polarized quarks in a transversely polarized nucleon. The expected asymmetries from the leading-order calculations and Monte Carlo studies are in the range of 2 to 10%, depending on the kinematics and on the models used for the PDFs. The  $x_B$ ,  $z$  and  $P_T$  dependences of the TTSAs will be studied in a wide kinematic range.

A total of 100 days of beam time is requested for this experiment.

# Contents

<b>1</b>	<b>Introduction</b>	<b>5</b>
<b>2</b>	<b>Theory and Motivation</b>	<b>9</b>
2.1	Transversely Polarized Target . . . . .	12
2.2	Present Experimental Results on Spin-Azimuthal Asymmetries . . . .	13
2.3	Scientific Case and Recent Developements in the Kaon Sector . . . .	16
2.3.1	The flavor-dependence of Boer-Mulders and Collins functions .	21
2.3.2	Transverse momentum dependence of partonic distributions .	22
2.3.3	Vector meson contribution . . . . .	23
<b>3</b>	<b>Experimental Situation</b>	<b>24</b>
3.1	The HERMES and COMPASS Experiments . . . . .	24
3.2	JLab Proposals . . . . .	24
<b>4</b>	<b>A Dedicated SIDIS Experiment with a Transversely Polarized Target and CLAS12</b>	<b>24</b>
4.1	The CLAS12 Configuration . . . . .	25
4.1.1	The HD-Ice Transversely Polarized Target . . . . .	25
4.1.2	A Magnetic System for the CLAS12 Transverse Target . . . .	27
4.1.3	Target Polarization Measurements . . . . .	31
4.1.4	The Impact of Møller Scattering . . . . .	32
4.2	The CLAS12 Particle Identification . . . . .	32
4.3	The CLAS12 RICH detector . . . . .	34
4.3.1	Preliminary Monte Carlo results . . . . .	36
4.4	The Measurement . . . . .	40
4.4.1	Event Identification, Reconstruction, and Acceptances . . . .	40
4.4.2	Acceptance and Data Analysis . . . . .	42
4.4.3	Count Rates and Statistical Errors . . . . .	42
4.4.4	Systematic Errors . . . . .	43
4.5	Projected Results . . . . .	45
4.6	Fourier Transformed Cross Sections . . . . .	52
<b>5</b>	<b>Summary and Beam Time Request</b>	<b>55</b>

# 1 Introduction

One of the main objectives of the Jefferson Lab upgrade is the understanding of the internal structure of the nucleon and nucleus in terms of quarks and gluons, the fundamental degrees of freedom of Quantum Chromodynamics (QCD). The partonic structure of hadrons beyond the collinear PDFs, or 3D structure of the nucleon, can be described by two new types of parton distributions: the transverse momentum dependent parton distributions (TMDs) [1, 2, 3, 4, 5, 6, 7, 8], and the generalized parton distributions (GPDs) [9, 10, 11, 7, 12, 13, 14, 15].

The ultimate knowledge of finding a single parton inside a hadron – involving both momentum and space information – can be encoded in the phase-space distributions of quantum mechanics, such as the Wigner quasi-probability distribution  $W(k, b)$ , whose integration over the parton spatial dependence ( $b$ ) leads to the TMDs, while its integration over transverse momentum ( $k$ ) provides the parton’s spatial distribution that is relevant to the GPDs. Understanding both the momentum and spatial distribution of a parton inside a hadron in terms of the more general Wigner distributions could be the central object of future studies on partonic structure. The concept of Wigner distributions in QCD for quarks and gluons was first explored in Refs. [16, 7], introducing the definition of a Wigner operator whose matrix elements in the nucleon states were interpreted as distributions of the partons in a six-dimensional space (three position and three momentum coordinates). The link with GPDs was exploited to obtain three-dimensional spatial images of the proton which were interpreted as charge distributions of the quarks for fixed values of the Feynman variable  $x$ .

Significant progress has been recently made in understanding the role of partonic initial and final state interactions [17, 18, 19]. The interaction between the active parton in the hadron and the spectators leads to gauge-invariant transverse momentum dependent (TMD) parton distributions [17, 18, 19, 20, 21, 22]. Furthermore, QCD factorization for semi-inclusive deep inelastic scattering at low transverse momentum in the current-fragmentation region has been established in Refs. [23, 24]. This new framework provides a rigorous basis to study the TMD parton distributions from SIDIS data using different spin-dependent and spin-independent observables. TMD distributions (see Table 1) describe different spin-spin and spin-orbit correlations in the momentum space [25, 8, 26, 27]. Knowledge of TMDs is also crucial for understanding phenomena in high energy hadronic scattering processes, such as, the single transverse spin asymmetries [17, 28, 18, 19, 20, 29].

The diagonal elements of Table 1 are occupied by the three fundamental leading-twist parton distribution functions: the *momentum*, the *helicity* and the *transversity* distributions. They are all needed for a complete description of the collinear nucleon structure, and are the only ones that survive after integration over the intrinsic transverse momentum. The Sivers function ( $f_{1T}^\perp(x, k_T^2)$ ), which describes the difference between the probability to find a quark with lightcone momentum fraction  $x$

and transverse momentum  $k_T$  inside a hadron polarized transversely to its momentum direction, and the one where the polarization points in the opposite direction, has been phenomenologically extracted by several groups, mainly from analyzing the azimuthal distribution of a single hadron in SIDIS [30, 31, 32, 33]. However, in the case of positive hadrons, where a signal has been seen, the measurements of HERMES [34] and COMPASS [35] experiments are only marginally compatible: the asymmetries measured by COMPASS are somewhat smaller, and seem to indicate an unexpected dependence on  $W$ , the mass of the hadronic final state. Significant differences observed between Sivers asymmetry measurements for pions and kaons still require new theory development and more precision measurements for kaons.

Important aspects of the TMD parton distributions, such as gauge invariance, the role of gauge links, and universality, have been explored in recent years [18, 19, 20, 22, 29, 36, 37, 38]. Like the PDFs, the definition of TMDs is closely connected to the factorization of physical cross sections, and it is necessary for the TMDs to include all leading power long-distance contributions to the physical cross sections if they can be factorized. All leading power collinear gluon interactions are summed into the gauge links in the definition of the TMDs. It is the gauge link that makes the TMDs gauge invariant and provides the necessary phase for generating a sizable single transverse spin asymmetry (SSA) in SIDIS and Drell-Yan processes [17, 28, 18, 19, 20, 22]. However, unlike the PDFs, which are universal, the TMDs could be process dependent due to the fact that the initial-state and final-state collinear gluon interactions are summed into two different gauge links. That is, the TMDs extracted from SIDIS could be different from those extracted from Drell-Yan processes because of the difference in gauge links.

Although the TMDs are not in general universal, it can be shown from the parity and time-reversal invariance of QCD dynamics that the process dependence of the spin-averaged as well as spin-dependent TMDs is only a sign, which was referred to as the parity and time-reversal modified universality [18, 29]. An important example of the modified universality is that the Sivers function extracted from the SIDIS measurements is opposite in sign from the Sivers function extracted from the Drell-Yan process. The test of the sign change of the Sivers function from SIDIS to Drell-Yan is a critical test of the TMD factorization and several DY proposals were approved to measure TMDs [39, 40] and perform that test [41]. The possibility of a node in the  $x$ -dependence of the Sivers function has been discussed in light of its importance for the experimental check of the sign change of the Sivers function between semi-inclusive DIS and the Drell-Yan process [42]. As the Sivers function describes a difference of probabilities it is not necessarily positive definite. Recent measurements of multiplicities and double spin asymmetries as a function of the final transverse momentum of pions in SIDIS at JLab [43, 44] suggest that transverse momentum distributions may depend on the polarization of quarks and possibly also on their flavor. Calculations of transverse momentum dependence of TMDs in different models [45, 46, 47, 48] and on lattice [49, 50] indicate that the dependence of the transverse

N/q	U	L	T
U	$\mathbf{f_1}$		$h_1^\perp$
L		$\mathbf{g_1}$	$h_{1L}^\perp$
T	$f_{1T}^\perp$	$g_{1T}^\perp$	$\mathbf{h_1} \quad h_{1T}^\perp$

Table 1: Leading-twist transverse momentum-dependent distribution functions.  $U$ ,  $L$ , and  $T$  stand for transitions of unpolarized, longitudinally polarized, and transversely polarized nucleons (rows) to corresponding quarks (columns).

momentum distributions on the quark polarization and flavor may be very significant. There are some indications that the transverse momentum dependence of the Sivers functions, important for comparison of Sivers function measurements from different processes and the corresponding collinear higher twist, may also not be trivial [51].

Recently it has been suggested, based on some quark models, that the pretzelosity TMD,  $h_{1T}^\perp$ , may also be related to the quark orbital angular momentum (OAM) [52, 53, 54, 55]

$$\mathcal{L}_z^q = - \int dx d^2k_\perp \frac{\vec{k}_\perp^2}{2M^2} h_{1T}^{\perp q}(x, \vec{k}_\perp^2). \quad (1)$$

The TMD  $h_{1T}^\perp$ , which describes the distribution of transversely polarized quarks in a transversely polarized nucleon, corresponds to the amplitude where the nucleon and active quark longitudinal polarizations flip in opposite directions, involving therefore a change by two units of OAM between the initial and final nucleon states. It was shown that in a gauge theory, in general,  $\mathcal{L}_z^q$  (see *e.g.* [56]) may not be related to the total quark contribution to the nucleon spin from a combination of GPDs from Ji's sum-rule [57].

Another interesting TMD distribution function accessible in studies with transversely polarized nucleons is the *worm-gear*  $g_{1T}^\perp$ . It describes the probability to find longitudinally polarized quarks in a transversely polarized nucleon. Noteworthy, it is the only TMD function not affected by initial- or final-state interactions as it is neither chiral-odd nor T-odd. It can be accessed, in conjunction with the spin-independent fragmentation function  $D_1$ , in double-spin asymmetries with a longitudinally polarized beam and a transversely polarized nucleon.

There have been many interesting model studies recently, see for example [58, 54, 59, 60, 47, 26]. These models and their calculations could play a very important role as a first step to describe the experimental observations, to give an intuitive way to connect the physical observables to the partonic dynamics, and to provide key inputs to the partonic structure of the nucleon. This will help us to address the fundamental questions, such as how the quark spin and its orbital angular momentum contribute to the nucleon spin? More importantly, very exciting results of TMDs have come from recent lattice QCD calculations [49, 61, 50], indicating that spin-orbit correlations could change the transverse momentum distributions of partons. Model

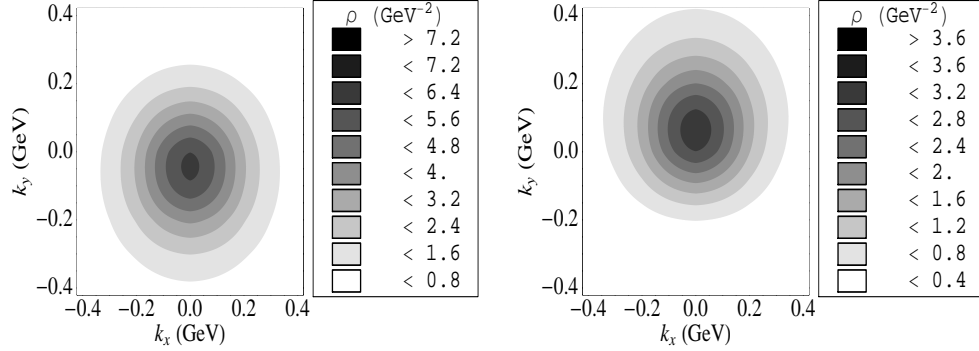


Figure 1: Spin density in the transverse-momentum plane for unpolarized quarks in a transversely polarized nucleon [60]. The left panel is for up quarks, and the right panel for down quarks.

calculations are consistent with lattice calculations and measurements at HERMES and COMPASS indicating opposite signs for the Sivers functions for  $u$  and  $d$  quarks (Fig. 1).

Similar correlations arise in the hadronization process. One particular case is the Collins  $T$ -odd fragmentation function  $H_1^\perp$  [62], describing fragmentation of transversely polarized quarks into unpolarized hadrons.

The off-diagonal TMD distributions for transversely polarized quarks arise from interference between amplitudes with left- and right-handed polarization states, and only exist because of chiral symmetry breaking in the nucleon wave function in QCD. Their study therefore provides a new avenue for probing the chiral nature of the partonic structure of hadrons.

We propose a high luminosity ( $10^{34} \text{ cm}^{-2}\text{s}^{-1}$ ) measurement of transverse target single-spin asymmetries in SIDIS using the CLAS12 detector in Hall B with an 11 GeV longitudinally polarized electron beam and the transversely polarized HD-Ice target. The main goal of this proposal will be the study of the  $x_B$  and  $P_T$  dependences of transverse target single-spin asymmetries (SSAs) and double-spin asymmetries (DSAs).

The proposed measurements are essential for the study of the transverse momentum-dependent distributions and, when combined with already approved CLAS12 measurements with unpolarized and longitudinally polarized targets, will constrain all chiral-odd leading twist TMDs in the range of  $Q^2$  from 1 to 8  $\text{GeV}^2$ , and  $x_B$  from



0.05 to 0.6. One of the main focuses of the proposed measurement will be the transverse momentum dependence of the underlying TMDs, and in particular of the Sivers function. The same measurement will also provide important information on different sub-leading distribution functions [63, 64].

The CLAS12 detector will provide a unique opportunity to perform the measurements over a wide range of kinematics with a single experiment.

## 2 Theory and Motivation

In recent years, semi-inclusive deep inelastic scattering (SIDIS) has emerged as a powerful tool to probe the nucleon structure through measurements of single- and double-spin asymmetries [65, 66, 67, 68]. In contrast to inclusive deep inelastic lepton-nucleon scattering, where the transverse momentum is integrated out, these processes are sensitive to transverse momentum scales on the order of the intrinsic quark momentum. Measurements of SSAs in SIDIS provide access to a list of novel physics observables including transversity ( $h_1$ ) [1, 69] and the time-reversal odd Sivers distribution function ( $f_{1T}^\perp$ ) [70, 71, 17, 18, 19].

The SIDIS cross section can be decomposed in terms of Structure Functions [23, 8], each related to a specific azimuthal modulation:

$$\begin{aligned}
\sigma(\phi, \phi_S) \equiv \frac{d^6\sigma}{dx dy dz d\phi d\phi_S dP_{h\perp}^2} &= \frac{\alpha^2}{xyQ^2} \frac{y^2}{2(1-\epsilon)} \left( 1 + \frac{\gamma^2}{2x} \right) \\
&\left\{ F_{UU,T} + \epsilon F_{UU,L} + \sqrt{2\epsilon(1+\epsilon)} \cos\phi F_{UU}^{\cos\phi} + \epsilon \cos(2\phi) F_{UU}^{\cos(2\phi)} \right. \\
&\quad \left. + \lambda_e \sqrt{2\epsilon(1-\epsilon)} \sin\phi F_{LU}^{\sin\phi} \right. \\
&\quad \left. + S_L \left[ \sqrt{2\epsilon(1+\epsilon)} \sin\phi F_{UL}^{\sin\phi} + \epsilon \sin(2\phi) F_{UL}^{\sin(2\phi)} \right] \right. \\
&\quad \left. + S_L \lambda_e \left[ \sqrt{1-\epsilon^2} F_{LL} + \sqrt{2\epsilon(1-\epsilon)} \cos\phi F_{LL}^{\cos\phi} \right] \right. \\
&\quad \left. + |S_T| \left[ \sin(\phi - \phi_S) \left( F_{UT,T}^{\sin(\phi-\phi_S)} + \epsilon F_{UT,L}^{\sin(\phi-\phi_S)} \right) \right. \right. \\
&\quad \left. + \epsilon \sin(\phi + \phi_S) F_{UT}^{\sin(\phi+\phi_S)} + \epsilon \sin(3\phi - \phi_S) F_{UT}^{\sin(3\phi-\phi_S)} \right. \\
&\quad \left. + \sqrt{2\epsilon(1+\epsilon)} \sin\phi_S F_{UT}^{\sin\phi_S} + \sqrt{2\epsilon(1+\epsilon)} \sin(2\phi - \phi_S) F_{UT}^{\sin(2\phi-\phi_S)} \right. \\
&\quad \left. + |S_T| \lambda_e \left[ \sqrt{1-\epsilon^2} \cos(\phi - \phi_S) F_{LT}^{\cos(\phi-\phi_S)} + \sqrt{2\epsilon(1-\epsilon)} \cos\phi_S F_{LT}^{\cos\phi_S} \right. \right. \\
&\quad \left. \left. + \sqrt{2\epsilon(1-\epsilon)} \cos(2\phi - \phi_S) F_{LT}^{\cos(2\phi-\phi_S)} \right] \right\}, \tag{2}
\end{aligned}$$

where  $\lambda_e$  refers to the helicity of the electron beam,  $S_L$  and  $S_T$  to the longitudinal and transverse polarization of the target nucleons (with respect to the direction of

the virtual photon), and  $\epsilon$  to the ratio of the longitudinal and transverse photon fluxes, which is determined by the kinematics of the lepton. Here,  $q = l - l'$  is the four-momentum of the virtual photon,  $Q^2 = -q^2$ ,  $x = Q^2/2(Pq)$ ,  $y = (Pq)/(Pl)$ ,  $\phi_S$  is the azimuthal angle of the transverse spin in the scattering plane, and  $P$  is the initial nucleon momentum. The azimuthal angle  $\phi$  is defined as the angle between the scattering plane, formed by the initial and final momenta of the electron, and the production plane, formed by the transverse momentum  $P_T$  of the observed hadron and the virtual photon (Fig. 2).

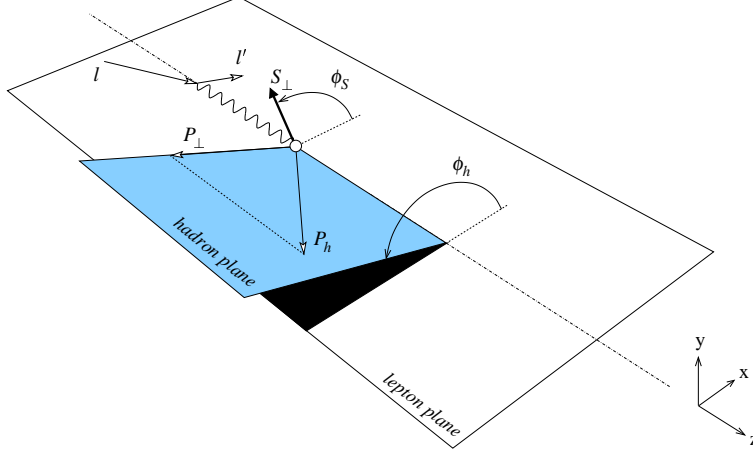


Figure 2: The SIDIS kinematics.

The subscripts in the *structure functions*  $F_{UT,UL,LT}$ , specify the beam (first index) and target (second index) polarization ( $U, L, T$  for unpolarized, longitudinally and transversely polarized targets, and  $U, L$  for unpolarized and longitudinally polarized beam).

At leading twist there are eight contributions related to different combinations of polarization states of the incoming lepton and the target nucleon. The structure functions factorize into TMD parton distribution and fragmentation functions, and soft and hard parts [23]. For example,  $F_{UT}^{\sin(\phi+\phi_S)}$  can be written as

$$F_{UT}^{\sin(\phi+\phi_S)} = \int \frac{\vec{p}_\perp \cdot \hat{\vec{P}}_T}{M} \times h_1(x_B, k_\perp) H_1^\perp(z, p_\perp) S(\vec{\lambda}_\perp) H_{UT}(Q^2) . \quad (3)$$

The hard factor,  $H_{UT}$ , is calculable in pQCD, and the soft factor  $S(\vec{\lambda}_\perp)$  comes from soft gluon radiation and is defined by a matrix element of Wilson lines in the QCD vacuum [23]. The integral symbol represents integration over the transverse momentum of the initial,  $k_\perp$ , and scattered  $p_\perp$  partons and the soft gluon momentum  $\vec{\lambda}_\perp$  [72]. The distribution ( $h_1$ ) and fragmentation ( $H_1^\perp$ ) functions involved depend

on the fraction of the proton momentum carried by the struck quark,  $x_B$ , and of the virtual photon momentum carried by the final state hadron,  $z$ , as well as on the corresponding transverse momenta  $k_\perp$  and  $p_\perp$ .

The TMDs define the probability density of finding a (polarized) quark with longitudinal momentum fraction  $x$  and transverse momentum  $k_T$  inside polarized and unpolarized nucleons. For example, the probability of finding an unpolarized quark with longitudinal momentum fraction  $x$  and transverse momentum  $\vec{k}_T$  inside a transversely polarized target is given by:

$$\Phi^q(x, \vec{k}_T; S) = f_1^q(x, \vec{k}_T^2) - \frac{(\hat{P} \times k_T) S_T}{M} f_{1T}^{\perp q}(x, \vec{k}_T^2). \quad (4)$$

The Sivers contribution, being leading twist, is expected to survive at higher  $Q^2$ , and this can be tested with CLAS12. At large hadron transverse momentum, *i.e.*  $P_{h\perp} \gg \Lambda_{\text{QCD}}$ , the transverse-momentum dependence of the various factors in the factorization formula [23] may be calculated from perturbative QCD. Following arguments in Ji-Qiu-Vogelsang-Yuan [73], the  $\sin(\phi - \phi_S)$  azimuthal asymmetry has the following behavior at  $\Lambda_{\text{QCD}} \ll P_{h\perp} \ll Q$ ,

$$\langle \sin \phi - \phi_S \rangle |_{P_{h\perp} \gg \Lambda_{\text{QCD}}} \propto \frac{1}{P_{h\perp}}. \quad (5)$$

The above result holds also when the transverse momentum is compatible with the large-scale  $Q$ . Measurement of the  $P_T$  dependence of the Sivers asymmetry will, thus, check the predictions of a unified description of SSA by Ji and collaborators [23, 73] and will study the transition from a non-perturbative to a perturbative description. The Sivers asymmetry for semi-inclusive deep inelastic scattering in the kinematic regions of CLAS12 is predicted to be significant ( $\sim 10\%$  at large  $P_T$ ) and tends to be larger in the large- $x$  and large- $z$  regions. Measurement of the  $P_T$ -dependence of the Sivers asymmetry provides access to the transverse momentum-dependence of the Sivers TMD and its moments. This, in particular, would allow one to determine the first moment of the Sivers function:

$$f_{1T}^{\perp(1)}(x) = \int d^2 \vec{k}_T \frac{\vec{k}_T^2}{2M^2} f_{1T}^{\perp(1)}(x, \vec{k}_T^2). \quad (6)$$

This moment has a direct connection to so-called soft gluon pole matrix elements [74, 22, 26], and, as a consequence, one may also get a direct connection to the large single spin asymmetries already observed in, for instance,  $p^\uparrow p \rightarrow \pi X$  at Fermilab [75] and at RHIC [76]. Making such a cross check is crucial to understand the various transverse single-spin phenomena in semi-inclusive reactions by means of perturbative QCD. The  $P_T$ -dependence will thus provide access to the  $k_T$ -dependence of the Sivers function, which may be relevant to resolve the so-called “sign mismatch”,

or the observed mismatch between the signs of the moment of the Sivers function extracted from SIDIS data and twist-3 calculations [51].

Studies of the shape of the proton indicate [77, 78] that for transversely polarized quarks in a transversely polarized nucleon, the shape of the nucleon is reminiscent of a pretzel. The distribution of transversely polarized quarks is described by the TMD  $h_{1T}^\perp$  and its magnitude will thus be related to the “pretzelosity” of the proton [77].

## 2.1 Transversely Polarized Target

For a transversely polarized target, several azimuthal asymmetries already arise at leading order. Four contributions related to the corresponding distribution functions were investigated in Refs. [62, 4, 3, 17, 19, 79]:

$$\begin{aligned}
\sigma_{UT}^{\sin\phi} &\propto S_T(1-y)\sin(\phi+\phi_S)\sum_{q,\bar{q}}e_q^2xh_1(x)H_1^{\perp q}(z) \\
&+ S_T(1-y+y^2/2)\sin(\phi-\phi_S)\sum_{q,\bar{q}}e_q^2xf_{1T}^{\perp q}(x)D_1^q(z) \\
&+ S_T(1-y)\sin(3\phi-\phi_S)\sum_{q,\bar{q}}e_q^2xh_{1T}^{\perp q}(x)H_1^{\perp q}(z) \\
\sigma_{LT}^{\cos\phi} &\propto \lambda_e S_T y(1-y/2)\cos(\phi-\phi_S)\sum_{q,\bar{q}}e_q^2xg_{1T}^q(x)D_1^q(z), \tag{7}
\end{aligned}$$

where  $y$  defines the fraction of electron momentum carried by the virtual photon. Here,  $D_1^q(z)$  and  $H_1^{\perp q}(z)$  represent the spin-independent and spin-dependent (Collins) fragmentation functions.

The leading-twist transversity distribution  $h_1$  [1, 69] and its first moment, the tensor charge, are as fundamental for understanding of the spin structure of the nucleon as are the helicity distribution  $g_1$  and the axial vector charge. The transversity distribution  $h_1$  is chirally odd, and there is no gluon transversity in the nucleon. For non-relativistic quarks it is equal to the helicity distribution  $g_1$ . Thus, it probes the relativistic nature of quarks and it has a very different  $Q^2$  evolution than  $g_1$ . The tensor charge is reliably calculable in lattice QCD with  $\delta\Sigma = \sum_f \int_0^1 dx (h_1^f - \bar{h}_1^f) = 0.562 \pm 0.088$  at  $Q^2=2 \text{ GeV}^2$ , which is twice as large as the value of the axial charge [80]. A similar quantity ( $\delta\Sigma \approx 0.6$ ) was obtained in the effective chiral quark soliton model [81].

A detailed study of the  $x_B$ ,  $y$ ,  $z$ , and  $P_T$  dependences as a function of the azimuthal angle  $\phi$  will allow the separation of contributions from different mechanisms. Combining the data from CLAS12 with a transversely polarized target with data from CLAS and CLAS12 with unpolarized and longitudinally polarized targets, will provide a complete set of measurements required for the separation of all eight leading-twist TMD distribution functions shown in Table 1.

It is important to note that both  $\pi^+$  and  $\pi^-$  azimuthal moments may have significant contributions from exclusive vector meson production. The fraction of  $\pi^+$  in the single pion sample, coming from exclusive  $\rho^0$  decays, is significant at large  $z$  and at small  $x$ . The two-pion data from this experiment will allow us to extract exclusive two-pion asymmetries and estimate their contribution to the single pion SSA.

A full program to extract TMDs from measurements requires coverage of a large kinematic range in  $x_B$ ,  $z$ , and  $P_T$ , along with very good hadron identification (to allow *flavor tagging*), and the use of polarized beam and polarized targets (both longitudinal and transverse polarizations).

## 2.2 Present Experimental Results on Spin-Azimuthal Asymmetries

During the last few years, the first results on transverse SSAs have become available [66, 67, 68, 82, 35, 83]. HERMES and COMPASS measurements for the first time directly indicated significant azimuthal moments generated both by the Collins and the Sivers effects.

The extraction of the transversity from  $A_{UT}^{\sin(\phi+\phi_S)}$  requires parametrizations for the unpolarized distribution functions along with approximations for the essentially unknown polarized Collins fragmentation function  $H_1^\perp$ . The Collins function for pions was calculated in a chiral invariant approach at a low scale [85]. It was shown that at large  $z$  the function rises much faster than previously predicted [86, 87] in the analysis using the HERMES data on target SSA. A significant asymmetry was measured recently by Belle [88, 89, 90], indicating that the Collins function is indeed large. The first extraction of the transversity distribution, together with the Collins fragmentation function, has been carried out recently [91, 84] through a global fit of the BELLE data from  $e^+e^-$  annihilation and the HERMES [66] and COMPASS [67, 68, 92] data on semi-inclusive DIS (see Figs. 3-4). Similarly, a recent extraction of the Sivers function for  $u$ ,  $d$ , and  $s$  flavors, also based on the SIDIS results from HERMES and COMPASS, is shown in Fig. 5. The data available, however, is not enough to make statistically significant predictions in the valence region, where the effects are large.

The effects related to orbital motion of quarks, and in particular the correlations of spin and transverse momentum of the quarks, play an important role especially in the valence region. It was shown that spin-orbit correlations may lead to a significant contribution to partonic momentum and helicity distributions [93] in the large- $x$  limit.

Significantly higher statistics from CLAS12 data, especially in the intermediate-to-large  $x_B$  region, will enable the extraction of the  $x_B$ ,  $z$  and  $P_T$  dependences for different azimuthal moments in a wide kinematic range, allowing the source of the observed SSA to be revealed, and the underlying distribution functions to be extracted. In particular, the combined analysis of the future CLAS12 data on  $A_{UT}$  and of the previous HERMES and COMPASS measurements in the small- $x_B$  domain, will provide information on the Sivers function, shedding light on the correlations between

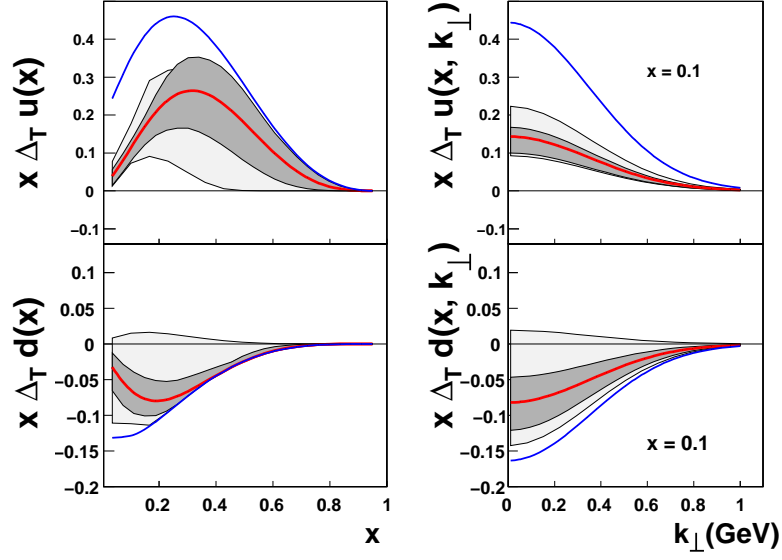


Figure 3: Transversity distribution functions for  $u$  and  $d$  flavors as extracted in [84].

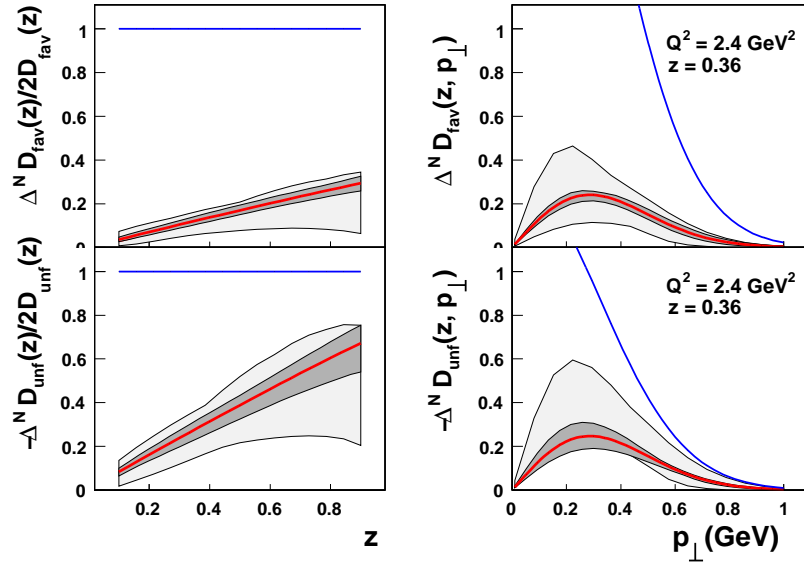


Figure 4: Favored and unfavored Collins fragmentation functions as extracted in [84].

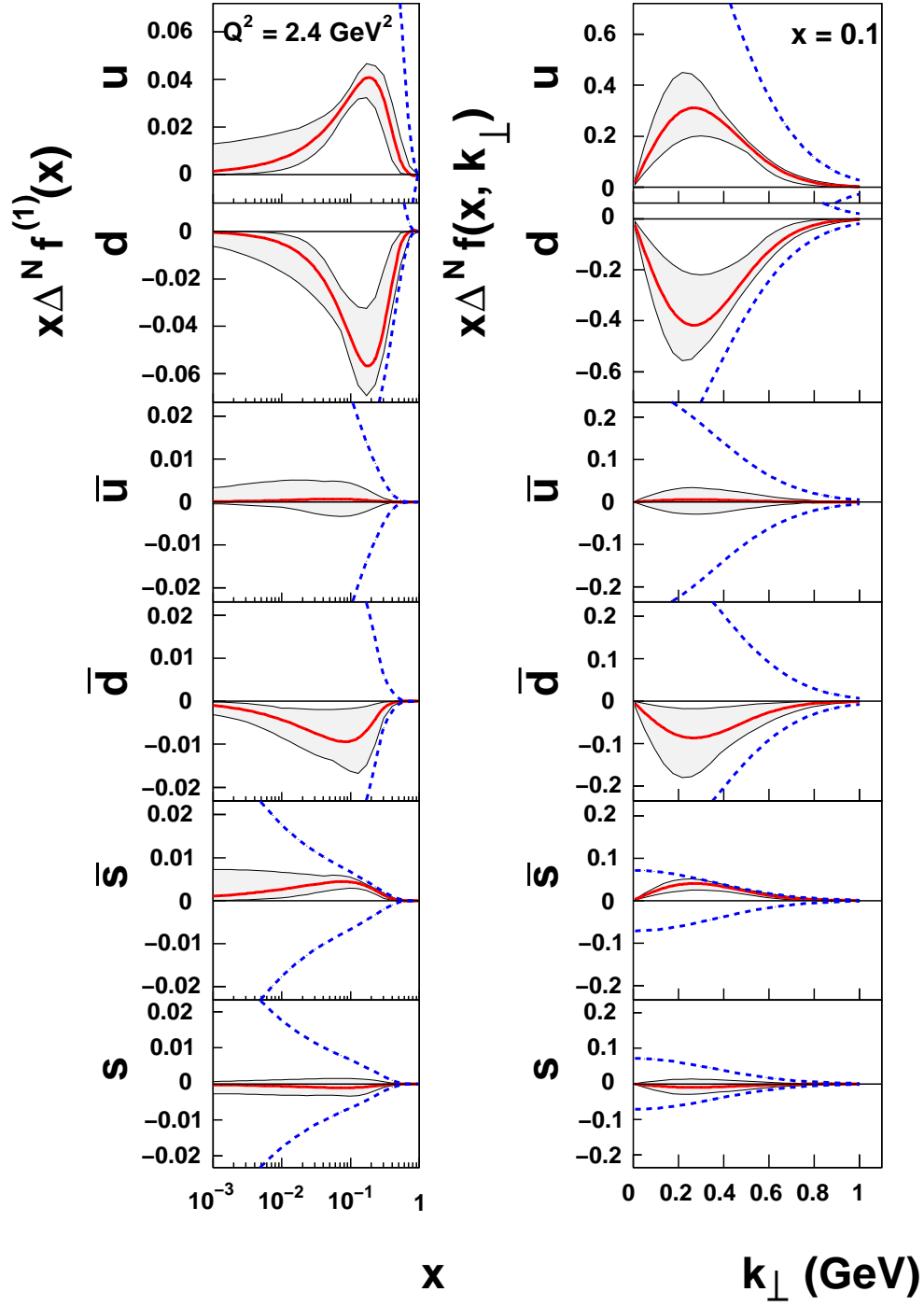


Figure 5: Sivers function for  $u$ ,  $d$ , and  $s$  flavors as extracted in [33].

transverse spin and transverse momenta of quarks.

SIDIS measurements with a joint use of a transversely polarized target and a longitudinally polarized beam provide access to the leading-twist TMD  $g_{1T}^q(x)$ , describing the distribution of longitudinally polarized quarks in a transversely polarized nucleon. This TMD appears at leading-twist in convolution with the unpolarized fragmentation function  $D_1^q(z)$  in a  $\cos(\phi - \phi_S)$  moment of the cross section (see eq. 7). Significant  $A_{LT}$  double-spin asymmetries were predicted recently for the JLab kinematics [94] (see Fig. 6), and are expected to be of similar magnitude at the CLAS12 kinematics.

The measurements of single and double spin asymmetries for pions and kaons in a large range of kinematic variables ( $x_B$ ,  $Q^2$ ,  $z$ ,  $P_T$ , and  $\phi$ ) combined with measurements with unpolarized targets, will provide detailed information on the flavor and polarization dependence of the transverse momentum distributions of quarks in the valence region and, in particular, on the  $x_B$  and  $k_T$  dependence of the leading TMD parton distribution functions of  $u$  and  $d$  quarks. Such measurements would allow for detailed tests of QCD dynamics in the valence region, complementing the information obtained from inclusive DIS. They would also serve as novel tools for exploring nuclear structure in terms of the quark and gluon degrees of freedom.

The combination of all 3 target polarization states (U, L, T) opens access to study of single- and double-spin asymmetries, involving essentially unexplored chiral-odd and time-reversal odd distribution functions, providing detailed information on the quark transverse momentum and spin correlations [62, 3, 4, 28, 95]. The list includes transversity [1, 69], Sivers [70, 17, 18, 19], “pretzelosity” [4],  $g_{1T}^q(x)$  [96], and Collins [62] functions.

## 2.3 Scientific Case and Recent Developements in the Kaon Sector

A comprehensive study of the nucleon structure should consider the role of the quark flavor. The use of different targets in conjunction with the detection of various hadrons in the final state provide access to statistical information about the flavor of the struck quark. In particular, kaons provide enhanced sensitivity on strangeness in the matter (partonic sea of the nucleon) and in the vacuum (through fragmentation). Kaon detection is generally challenged by the about one order of magnitude larger flux of pions. Thus very little is known about the spin-orbit correlations related to the strange quark. Only recently dedicated measurements have become available and, despite the limited statistical accuracy, in most of the cases they show surprising results.

In high-energy hadron-hadron collisions, large single-spin asymmetries have been measured since the eighties at large rapidities (positive Feynman- $x$ ) which are opposite in sign for opposite charge pions, see Fig. 7. This is not the case for charged kaons, whose SSA are recently measured to be non zero and of the same sign up to 200 GeV in center-of-mass energy [97, 98]. In SIDIS, precise hadron identification



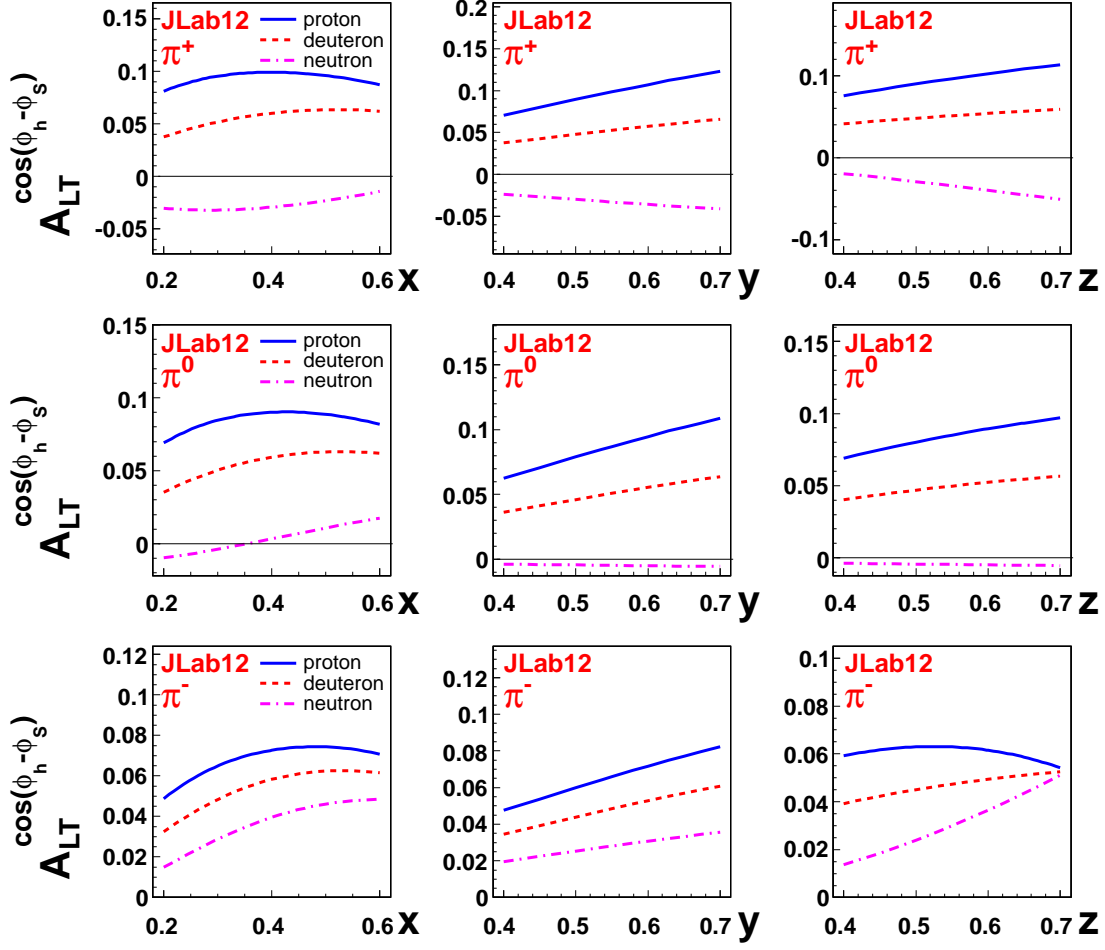


Figure 6: Predicted dependence of  $A_{LT}^{\cos(\phi_h - \phi_s)}$  on  $x$ ,  $y$  and  $z$  with  $|\mathbf{P}_{T,min}| = 0.5$  GeV/c for CLAS12 kinematics.

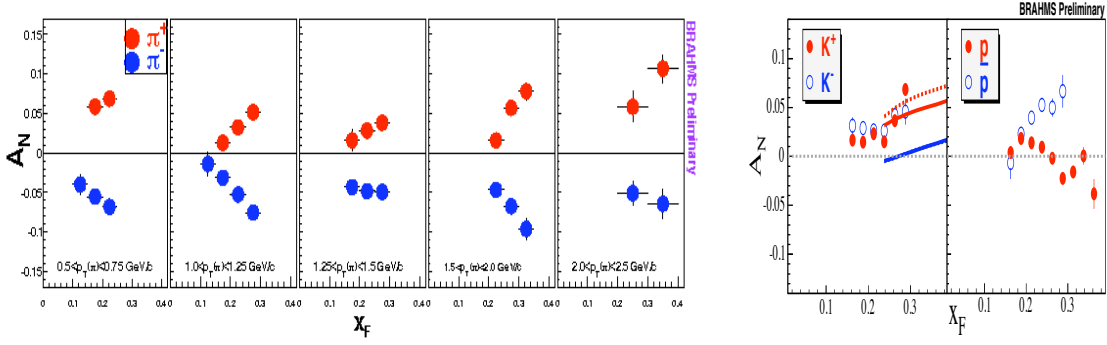


Figure 7: Single spin asymmetries for identified hadrons in proton-proton reactions at 200 GeV center-of-mass energy [98].

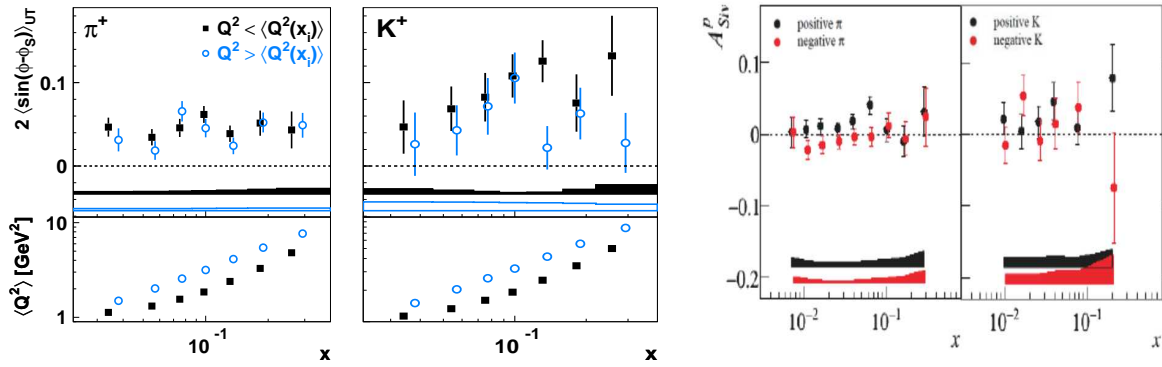


Figure 8: Sivers asymmetries measured for positive pions and kaons in two  $Q^2$  ranges at HERMES [34] (Left) and measured for identified charged hadrons at COMPASS [99] (Right).

has been exploited only by the second generation experiments. The Sivers effect, proposed as a possible explanation of the SSA in hadron-hadron collisions, generates SSA in SIDIS reactions for positive kaons which are found larger than for positive pions, see Fig. 8. The difference concentrate at low- $Q$ , a possible indication of the presence of higher-twist effects in the kaon sector [34]. The results for negative kaons are not conclusive due to the limited statistics [99].

The Collins asymmetry has been measured to be non-zero and opposite in sign for opposite charge pions, see Fig. 9. This is an indication that favored and unfavored Collins FF are opposite but of similar magnitude, a result compatible with the fragmentation-function measurement at  $e^+e^-$  machines [88, 101]. The SSA for positive kaons is similar to that of positive pions in sign and magnitude, a result compatible with the dominance of the  $u$ -flavor in lepto-scattering over a proton target.

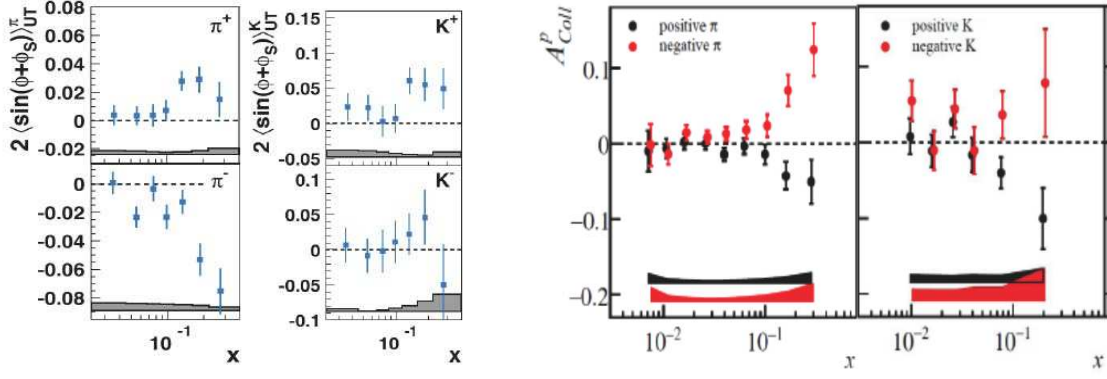


Figure 9: Collins asymmetries measured for identified charged hadrons at HERMES [82] (Left) and COMPASS [99] (Right).

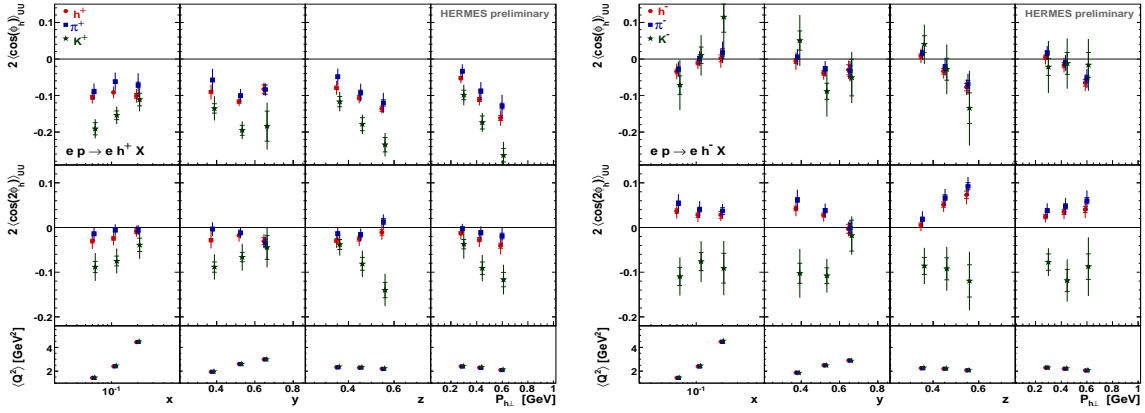


Figure 10: Azimuthal asymmetries in unpolarized SIDIS for identified hadrons [100].

However at HERMES, the signal for  $\pi^-$  and  $K^-$  are found to follow a different behavior, the former being large and negative, the latter being basically compatible with zero with a hint to be positive [82]. The result would be interesting since the  $K^-$  has no valence quarks in common with the target proton and sea quark transversity is expected to be small, thus  $K^-$  brings specific sensitivity on rank-2 Collins FF. Note that the knowledge of the Collins function has an impact on the extraction of all the chirally-odd TMD parton distributions. The result for  $K^-$  is still controversial, since COMPASS data [99] can not prove or disprove it, although seem to not support the same finding, see Fig. 9. The issue can be solved only by novel high-precision experiments.

Azimuthal asymmetries in unpolarized SIDIS cross-section are generated by the Cahn and Boer-Mulders effects, but may get not-negligible contributions from quark-gluon-quark correlators (pure sub-leading twist terms). Only recently preliminary SIDIS results become available with hadron identification or charge separation. Opposite-charge pion signals show unexpected large differences which can be related to the peculiar flavor dependence of the Collins FF entering the Boer-Mulders term [102]. These reflect in analogous differences for opposite-charge unidentified hadrons, dominated by the pion subsample [103]. The kaon results are definitely surprising, showing  $\cos 2\phi$  asymmetries much larger than pions but of the same sign for both charges [100], see Fig. 10. These asymmetries arise at leading-twist due to a convolution of Boer-Mulders with Collins functions, thus bring important piece of information on these two mechanisms. The sub-leading twist terms may also play a non-negligible role. The  $\cos\phi$  asymmetry gets contributions only at sub-leading twist and can be used to constrain the related terms. It shows a  $K^+$  signal larger than  $\pi^+$  but a  $K^-$  signal compatible with  $\pi^-$ . The kaon signals are a challenge for the present understanding of the underlying physics processes. Any explanations is not possible without a disentanglement of the different contributions, possible only with high-precision mapping of the kinematical dependences.

The surprising and controversial pattern of TMDs results for kaons is an indication of a non trivial role of the sea quarks in the nucleon, or of a peculiar behaviour of the fragmentation mechanism in the presence of strange quark. Moreover a hint exists that kaons provide enhanced sensitivity on higher-twist effects [34]. The interpretation would become possible only in the presence of high-luminosity large-acceptance experiments able to explore the relevant kinematic dependences in conjunction with an efficient hadron identification. Examples of wanted informations are a precise  $Q$ -dependence to isolate higher-twist effect and an extended  $P_{h\perp}$ -dependence to map the transient between perturbative and non-perturbative regime.

Nothing is known about polarization dependent FF (i.e. Collins) into kaons but an effort is being pursued to extract them from the large sample of data collected at B-factories [101, 104]. Very precise information on the fragmentation process is anticipated in the next future thanks to the approval of Super B-factories. The detailed study can be completed only by SIDIS measurements which constrain FF at much

lower center-of-mass energy with specific flavor sensitivity (not accessible in  $e^+e^-$  reactions). The detailed knowledge of the fragmentation process would reflect on the precise determination of parton distributions only at experiments with enough statistical precision and flavor sensitivity, like CLAS12 with a RICH detector dedicated to hadron identification.

The goal of our proposed experiment is to gather a data set on kaon SIDIS in the region  $0.1 \leq x \leq 0.8$ ,  $0 \leq P_T \leq 1.2$ , and  $0.2 \leq z \leq 0.8$ . Global analysis of the data combined with the analogous measurement approved with pions and polarized target data [105] will provide access to the flavor-decomposition of TMDs.

### 2.3.1 The flavor-dependence of Boer-Mulders and Collins functions

So far no experimental information is available about the Collins fragmentation function for kaons. Recent direct calculations of kaon Collins function [106] indicated that it may be comparable with pion Collins function. HERMES measurements of the Collins asymmetry for pions and kaons, though, with large uncertainties, indicate that the differences may be significant [82].

Pions and kaons are both Goldstone bosons of chiral symmetry breaking. In the chiral limit one has

$$\lim_{m_K \rightarrow 0} \frac{H_1^{\perp(1/2)a/K}}{D_1^{a/K}} = \lim_{m_\pi \rightarrow 0} \frac{H_1^{\perp(1/2)a/\pi}}{D_1^{a/\pi}}, \quad (8)$$

where  $H_1^{\perp(1/2)}$  means integration over the transverse momentum weighted with  $k_T$ .

Simultaneous measurements of the Boer-Mulders asymmetry for pions and kaons on proton and deuteron targets will provide an independent measurement of ratios of Collins functions of pions and kaons, providing complementary measurements to  $e^+e^-$  annihilation. Thanks to the different center-of-mass energy of fixed-target with respect collider experiments, the measurements can be used to test the evolution properties of the Collins function. That measurement will also provide a check of chiral limit prediction, where that ratio is expected to be at unity. With the knowledge of the Collins function, one can study all involved TMD distributions.

Measurement of the fraction coming from the Collins fragmentation of transversely polarized quarks in the unpolarized nucleon will require separation of other contributions, and in particular those due to the Cahn effect. Although, preliminary results from HERMES indicate that the Cahn contribution is not dominant in  $\cos 2\phi$  as was expected before [30]. In order to extract the contribution related to the Collins fragmentation one needs a reliable calculation of the kinematical corrections. Perturbative QCD contributions (at order  $\alpha_s$  and possibly  $\alpha_s^2$ ) to the kinematical  $\cos \phi_h$  and  $\cos 2\phi_h$  asymmetries also have to be evaluated. Such a study shows that the parton model with TMD DFs and FFs dominates at  $P_T$  values below 1 (GeV/c) [30].

TMD	$\langle k_T \rangle$ in GeV	$\langle k_T^2 \rangle$ in GeV <sup>2</sup>	$\frac{4\langle k_T \rangle^2}{\pi\langle k_T^2 \rangle}$	$\frac{\langle k_T^2 \rangle}{\langle k_{Tf_1}^2 \rangle}$
$f_1$	0.239	0.080	0.909	1.00
$g_1$	0.206	0.059	0.916	0.74
$h_1$	0.210	0.063	0.891	0.79
$g_{1T}^\perp$	0.373	0.176	1.007	2.20
$h_{1L}^\perp$	0.373	0.176	1.007	2.20
$h_{1T}^\perp$	0.190	0.050	0.919	0.63

Table 2: Predictions for the transverse momentum dependence of the T-even TMDs from the constituent quark model [47]. (Left) The mean transverse momenta and the mean square transverse momenta: if the transverse momenta in the TMDs were Gaussian, then the result for the ratio in the last row would be unity. (Right) Mean square transverse momenta of T-even TMDs in units of the mean square transverse momenta of  $f_1$ , denoted as  $\langle k_{Tf_1}^2 \rangle$ . These ratios are considered to be a more robust model prediction.

### 2.3.2 Transverse momentum dependence of partonic distributions

The width for different partonic distributions can be different. For example values for different T-even partonic distributions, computed [59] in the constituent quark model [47], are listed in Table 2. Values normalized to the width of the unpolarized distribution function are listed in the same Table.

A common assumption is the Gaussian ansatz for the transverse momentum dependence of distribution and fragmentation functions with the average  $P_{h\perp}$  of hadrons produced in SIDIS given by

$$\langle P_{h\perp}(z) \rangle = \frac{\sqrt{\pi}}{2} \sqrt{z^2 \langle k_T^2 \rangle + \langle p_T^2 \rangle}. \quad (9)$$

In the approximation of flavor and  $x$  or  $z$ -independent widths, a satisfactory description of HERMES deuteron data on average  $P_{h\perp}$  [107] was obtained [108] with

$$\langle k_T^2 \rangle = 0.33 \text{ GeV}^2, \quad \langle p_T^2 \rangle = 0.16 \text{ GeV}^2. \quad (10)$$

Numerically very similar results were obtained in Ref. [30] from a study of EMC data [109] on the Cahn effect. Although the ansatz seems to describe the present available data sets [58], it has to be considered an approximation which is not necessarily valid and most of the models do not base on it.

The unpolarized azimuthal moment in kaon lepto-production will be studied as a function of  $P_{h\perp}$ , in different bins in  $x, z$ , and  $Q^2$ , and complemented with the analogous measurements for pions. These measurements will provide access to widths in

transverse momentum of different underlying partonic distributions, like the number density  $f_1$  and the Boer-Mulders  $h_1$ , and to their flavor dependence.

This measurements, in conjunction with the study of hadron multiplicities in a large range of kinematic variables ( $x_B$ ,  $Q^2$ ,  $z$ ,  $P_{h\perp}$ ), will provide important input for the flavor decomposition of the transverse momentum dependence of all the others TMDs from polarized measurements.

### **2.3.3 Vector meson contribution**

One of the main sources of uncertainties for pions is the fraction of pions coming from vector meson decays. Since the Collins asymmetry has a significant dependence on the type of a produced hadron, pions produced from rho decays will have very different moments compared to direct pions. This makes measurements with kaons, which have a much smaller contribution from vector meson production, very important in understanding the underlying dynamics of the part of measured asymmetries due to Collins fragmentation mechanism

## 3 Experimental Situation

### 3.1 The HERMES and COMPASS Experiments

Target spin asymmetries have been published by the HERMES Collaboration on the proton [66, 34, 82] and the COMPASS collaboration on deuterium and proton targets [67, 35]. Kinematics at HERMES and in particular at COMPASS is limited to relatively low  $x_B$ , where the spin-orbit correlations are not expected to be large. Projected statistical errors for this proposal are shown in Section 4.5.

### 3.2 JLab Proposals

At Jefferson Lab there are two closely-related proposals approved to measure SSA with a transversely polarized  $^3\text{He}$  target in Hall-A [110, 111, 112]. The data from this experiment is complementary to the proposed CLAS12 measurement with transversely polarized hydrogen and deuterium targets. The large acceptance of CLAS12 will allow measurements of SIDIS pions over a wide range in  $x, Q^2$  and hadron transverse momenta, where the spin-orbit correlations and corresponding TTSA's are expected to be significant. A crucial advantage of proposed configuration is the negligible nuclear background, in particular for large  $P_T$ . The CLAS12 spectrometer equipped with a RICH detector, would allow a clean separation between pions, kaons and protons in a wide momentum range (1-10 GeV/c), thus providing flavor-tagging capabilities. In addition, wide acceptance and the capability to measure multi-particle final states will allow the simultaneous measurements of different exclusive vector mesons, important for understanding the background contributions to the Collins and Sivers asymmetries.

## 4 A Dedicated SIDIS Experiment with a Transversely Polarized Target and CLAS12

The main goal of the proposed experiment is to measure the  $x_B$  and  $P_T$  dependences of the target single- and double-spin asymmetries in the accessible kinematics (Fig. 11). The target single spin asymmetry (TSSA or  $A_{UT}$ ) will be calculated as:

$$A_{UT} = \frac{1}{fP_t} \frac{(N^+ - N^-)}{(N^+ + N^-)}, \quad (11)$$

where  $P_t$  is the target polarization (with respect to the electron beam direction),  $f$  is the dilution factor, i.e. the fraction of events from the polarized material of interest (H or D), and  $N^{+(-)}$  are the charge-normalized extracted number of  $ep^\uparrow \rightarrow ehX$  events for opposite orientations of the transverse spin of the target.



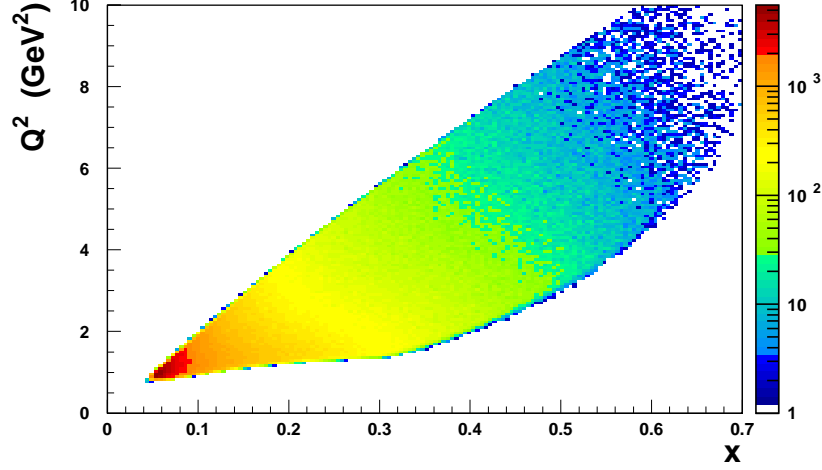


Figure 11: Kinematic coverage of CLAS12 with the transverse target.

The joint use of a transversely polarized target and a longitudinally polarized beam will also allow us to measure the double-spin asymmetry (TDSA or  $A_{LT}$ ) in the same kinematic region. These quantities are directly sensitive to the model descriptions of the corresponding TMDs and will be measured as:

$$A_{LT} = \frac{1}{fP_B P_t} \frac{(N^{+\uparrow} + N^{-\downarrow}) - (N^{+\downarrow} + N^{-\uparrow})}{(N^{+\uparrow} + N^{-\downarrow}) + (N^{+\downarrow} + N^{-\uparrow})}, \quad (12)$$

where  $P_B$  is the electron beam polarization, and  $N^{\pm\uparrow\downarrow}$  is the extracted number of  $ehX$  events for positive or negative helicities of the beam electrons and target polarizations.

The proposed experiment will provide statistically significant measurements of the kinematic dependences of the target TTSA and the TDSA in pion and kaon leptonproduction in SIDIS in the valence region.

## 4.1 The CLAS12 Configuration

### 4.1.1 The HD-Ice Transversely Polarized Target

The magnetic holding fields accompanying transversely polarized targets can deflect the electron beam and create challenging background conditions. A magnetic chicane is typically installed upstream of the target and arranged in such a way that

the target's magnetic field bends the electron beam back on axis [113]. However, bremsstrahlung created in the target material will be peaked along the direction of the incoming electrons, which will then be at several degrees to the detector axis depending on the holding field.

A transversely polarized target in a frozen-spin state, such as the HD-Ice target, requires only small holding fields, and greatly mitigates such background problems. Problems associated with beam deflection are virtually eliminated by the small holding fields and this potentially allows the target to be located even in the center of the detector, thus dramatically increasing the acceptance. In addition, the HD-Ice target has very limited dilution. The only unpolarizable nucleons are associated with the target cell and these can be sampled and subtracted in conventional empty-cell measurements. At the same time, the low  $Z$  results in a long radiation length and comparatively few bremsstrahlung photons.

The HD-Ice target developed at LEGS in Brookhaven and now moved from BNL to JLab, has been used quite successfully in photon beam experiments at BNL. The factors affecting target polarization are complex and intertwined; a direct test of the performance of polarized HD with electrons is essential and already approved and scheduled during the 2011/2012 run period in Hall B.

At BNL, HD target polarizations of 60% H and 35% D were achieved in photons experiments with spin-relaxation times in excess of a year, and polarizations are expected to be higher (75% H and 40% D) with the smaller diameter cells used at JLab. The deuterium polarization is particularly stable; spin-relaxation times of 2 months have been measured with only 0.01 T (100 gauss) holding field and 0.2 K. The projected D-decay time for a 0.04 T saddle coil, 0.12 m in length ( $\int BdL \approx 0.005$  T-m), is 7 months. Comparable H relaxation times require higher fields but should be possible with  $\int BdL = 0.050$  T-m, which is still about 30 times less than a dynamically polarized ammonia target.

Beam heating is considerably less in HD, as compared to Butanol, due to the lower  $Z$  and, unlike butanol, HD relaxation times are not such strong functions of temperature, so that long life-times are achievable up to about 0.7 K. Free radicals generated by electron bremsstrahlung will have randomly oriented polarizations. While their absolute number is small, they can generate polarization sinks within the target if the spin-diffusion time is short. This time constant has been indirectly measured at BNL by using RF to punch a local polarization hole within a highly polarized target. The rate at which this hole heals after the RF power is lowered reflects the in-diffusion of spin from other regions of the target. At 2 K, this measured spin-diffusion is 1 day for H but unmeasurably long for D (greater than a year). How much the H performance improves at lower temperatures is a matter for further study, but the extremely slow spin-diffusion for D already suggests that frozen-spin HD could maintain its deuterium polarization during electron experiments. The composition for a 10 cm solid HD-Ice target with 1.5 cm OD is shown in the Table 3. Frozen-spin HD-Ice, thus, provides a very attractive alternative for electron experiments in particular with

transversely polarized targets.

Table 3: HD-Ice target materials

Material	gm/cm <sup>2</sup>	mass fraction (%)
HD	0.735	82%
Al	0.155	14%
C <sub>2</sub> ClF <sub>3</sub>	0.065	4%

The insertion of a transverse target in CLAS12 requires a volume where the magnetic field of the main solenoid is shielded. In the shielded region a transverse target magnet can operate. In order to perform a preliminary feasibility study, a simplified main solenoid composed by a simple solenoidal coil was used. The dimensions of these coils are reported in Table 4.

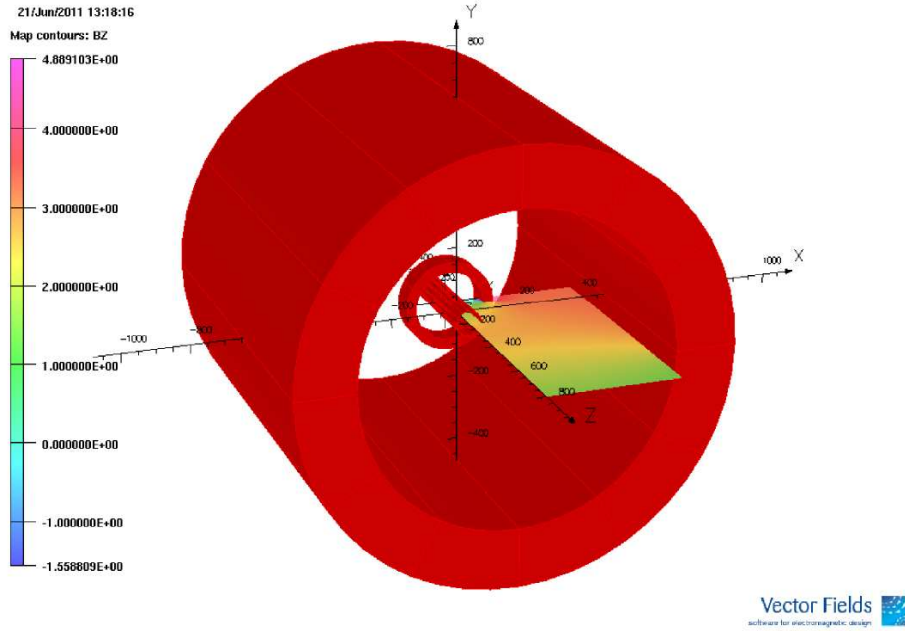


Figure 12: Magnet assembling for the HD-Ice target. Going outward from the beam line, there are the NMR coil of the target, the compensating solenoid and the central detector solenoid.

#### 4.1.2 A Magnetic System for the CLAS12 Transverse Target

The baseline of CLAS12 detector is based on two superconducting magnets. The 5 T main solenoid of the central detector allows particle momentum determination

in the backward region and constrains the large Moller background within the beam pipe. The large 2 T toroid magnet is used by the forward spectrometer as particle momentum analyzer.

To account for the possible sensitivity of HD-Ice to radiation damage, a luminosity of  $10^{34} \text{ cm}^{-2}\text{s}^{-1}$ , an order of magnitude lower than the one affordable with the CLAS12 detector, is here assumed. The Moller background is proportionally reduced and can be contained with a reduced solenoidal field: ongoing MC studies show that a 3 T field would be enough.

A magnetic configurations to shield the 3 T longitudinal field of the main solenoid in the target region has been studied. The HD-Ice target brings a thin superconducting solenoid for polarization measurement by NMR technique, able to provide a field of the order of 0.5 T. Larger fields are achievable by winding additional wire. In order to minimize the material budget inside the acceptance, an external solenoid is inserted at the place of the silicon vertex detector barrel. The coil is designed to allows a  $\pm 60$  degrees forward acceptance and to be contained within the micromegas barrel, see Fig. ???. This configuration provide enough clear solid angle to cover the forward spectrometer acceptance and part of the central detector which can then be used to detect recoiling protons in exclusive reactions (i.e. DVCS). The main parameters of the correction magnets are listed in Table 4. An ideal transverse magnet has been inserted in the magnetic assembly: it is a simple helical end (saddle) to supply 0.5 T transverse field in the target volume.

The main parameters of the magnet configuration for the HD-Ice target are listed in Table 4. The magnet assembling is shown in Fig. 12. The resulting magnetic field in the target volume is shown in Fig. 13. An important parameter is the uniformity of the transverse field holding the target polarization. The compensating coil is designed to reduce the longitudinal field to a negligible level in the center of the target. Due to the reduced length of the compensating coil, limited by the acceptance requirement, the compensation is not complete at the edges of the target. The unwanted longitudinal component reaches values up to 20% with respect the 1 T transverse component.

Experimentally the target transverse polarization is defined with respect the beam, whereas the component transverse to the virtual photon is the one relevant to theory. The angle between the beam and the virtual photon is approximately given by  $\sin \theta \approx \gamma \sqrt{1 - y}$  with  $\gamma = 2xM/Q$  and M the proton mass. As a consequence, the target spin naturally acquires a longitudinal component (with respect the virtual photon) which can be as high as 15%. The influence on transverse analyses has been studied in detail at HERMES, and quantified as negligible. This fix the order of magnitude of the longitudinal field component which can be tolerated into the target volume.

The load lines of the correction solenoids are shown in Fig. 14 where different superconducting wire performances are reported:

NbTi SUPERCON 0.229 wire used in the CLAS12 target,

NbTi SUPERCON wire used by the PAX experiment at FZJ (VSF/SSCI)

Table 4: Main parameters of the magnet assembling.

parameter	Central detector solenoid	compensating solenoid	NMR coil
inner radius (mm)	471	105	37.5
outer radius (mm)	650	135	38.5
length (mm)	1225	76	400
current density @ 3 T (A/mm <sup>2</sup> )	18.2	220	400

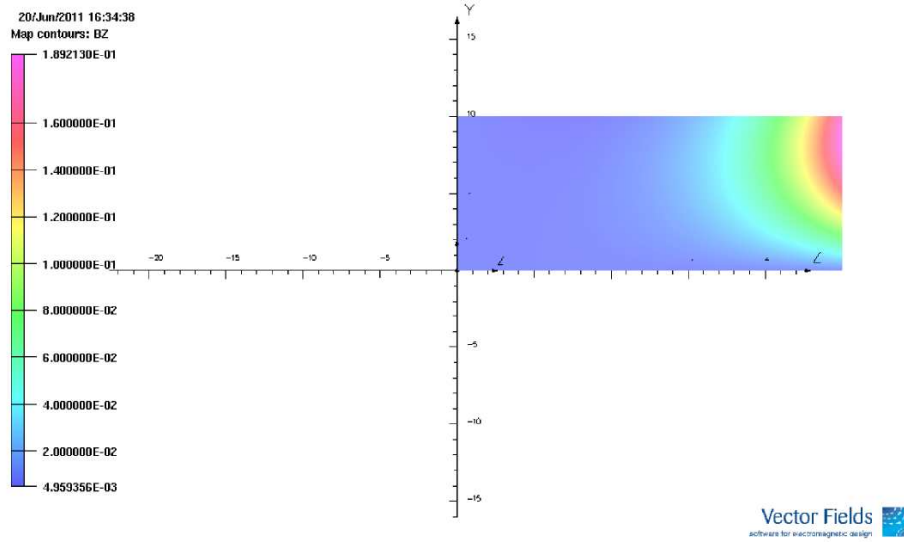


Figure 13: Magnetic field in the target volume (5 cm long cylinder of 1 cm diameter). Due to symmetry, only the downstream half of the cell is mapped. The color scale corresponds to the strength of the longitudinal field component of the field surviving the compensation, relative to the 1 T transverse field. The unwanted component is negligible at the center of the cell, but reaches values up to 20% at the edges.

NbTi BRUKER/EAS F54-(1.00)TV and OK54 wire by LUVATA/OUTOKUMPU

Nb3Sn SUPERCON wire is reported as well as a reference.

Considering the load line of the compensating solenoid and the working point at  $220 \text{ A/mm}^2$ , a good safety margin can be reached for the wires considered, i.e. for the OK54 wire the critical point is at almost  $500 \text{ A/mm}^2$  and the safety margin is above 40%.

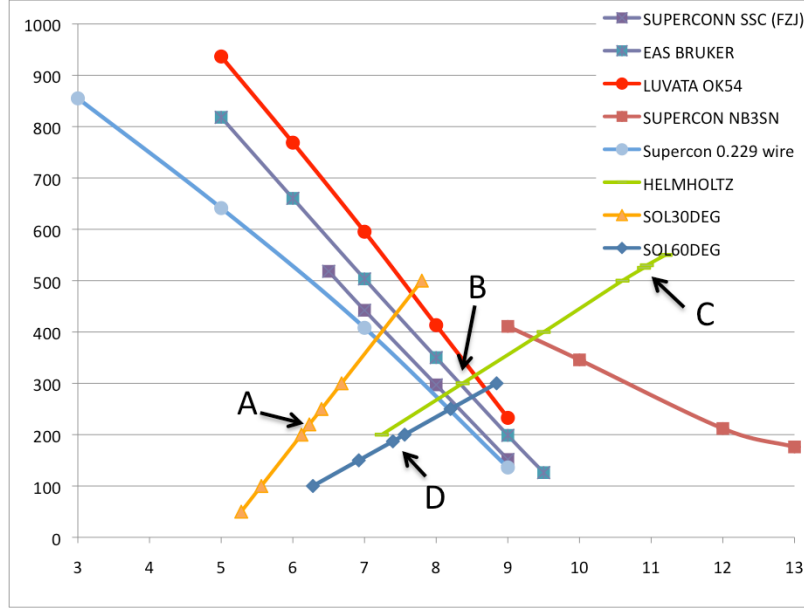


Figure 14: Load lines (curves increasing with field) as compared to the critical current (curves decreasing with field) of the superconducting wires. D is the working point for the 60-degrees acceptance correction solenoid. A, B and C working points refer to solutions not considered in this note.

In conclusion, a compensating solenoid in addition to the NMR coil of the HD-Ice target can be used to compensate the longitudinal field in the target volume. Both solenoids can be wound with existing standard commercial wires and work with a reasonable safety margin. The 60-degrees acceptance proposed solution is a first-order trade off between the requirement of uniform transverse field in the target (which would require longer solenoids) and the acceptance for large angle protons in exclusive measurements (which would require shorter solenoids). Work is in progress to optimize the performances of the system.

To avoid radiation damage to the target the beam will be rastered over the target surface in a spiral pattern. The beam position is measured indirectly by recording

the simultaneous currents of the raster magnet. These values can be used off-line to correct for effects of the raster on the vertex z-position. The raster magnets may be also used to give a small angle ( $\sim 0.1^\circ$ ) to the incident electron beam, so that beam at target center will be collinear with the z-axis to confine bremsstrahlung photons into the beam pipe.

#### 4.1.3 Target Polarization Measurements

There are four possible transverse combinations: (1) H and D both up, (2) H up/D down, (3) H down/D up, (4) H and D both down. Using the RF flipping of spins, one can switch between (1) and (4) or between (2) and (3) by simply rotating the field. The spins will follow, and this has 100% efficiency. Several samples with different orientations will be used in the experiment.

The target polarization will be measured with an NMR system [114, 115, 116]. Polarimetry for nuclear targets has been studied extensively at BNL. The In-Beam-Cryostat that will hold HD targets within CLAS12 will have a short saddle coil wound on top of a long solenoid. The saddle coil will maintain transverse spin orientations. Keeping this coil short will both reduce the  $BdL$  deflection of electrons, as well as minimize spin diffusion from radiation damage (by changing the Larmor frequency across the target). However, the fields associated with this coil will be too non-uniform for NMR measurements. Instead, the solenoid will be used for NMR polarization monitoring. The target spins will readily follow the field as the solenoid is energized and the saddle coil is ramped down. NMR data will be collected at the fields matching the Larmor frequencies, typically 0.15 T for H and 0.9 T for D, after which the saddle coil will be ramped up and the solenoid ramped down. We anticipate a total cycle time of about 15 minutes (limited by how fast the fields can be changed without quenching the magnets), enabling NMR data to be collected several times a day. The systematic uncertainties in HD polarization are about 4% (relative). The largest single factor (contributing 2.8% relative) is the differential uncertainty on the gain of a lock-in amplifier whose scale must be changed by many orders of magnitude between equilibrium-polarization measurements and high-polarization frozen-spin measurements. Separation of signal and background in the calibration measurements contributes at the 1% level.

An additional estimate of the product of target and beam polarizations,  $P_B P_t$ , will be done also off-line by comparing the well known  $ep$  elastic asymmetry

$$A_{theo} = - \frac{\cos \theta_\gamma \sqrt{1 - \epsilon^2} + (\frac{Q^2}{4M^2})^{-\frac{1}{2}} \sqrt{2\epsilon(1 - \epsilon)} \sin \theta_\gamma \cos \phi_\gamma \frac{G_E}{G_M}}{\epsilon(\frac{Q^2}{4M^2})^{-1} (\frac{G_E}{G_M})^2 + 1} \quad (13)$$

with the measured asymmetry

$$A_{meas} = \frac{N^+ - N^-}{N^+ + N^-} = \frac{P_B P_t \sigma_{et}}{\sigma_0} \equiv P_B P_t A_{theo}. \quad (14)$$

For the ratio  $\frac{G_E}{G_M}$ , we will use values from polarization transfer measurements [117], which are expected theoretically to have the same (small) two-photon corrections as  $A_{LT}$  measurements. On average, the uncertainty in  $A_{LT}$  due to  $G_E/G_M$  will be about 2% (relative). The measurements will consist of measuring both an electron and a proton, and imposing missing momentum and energy cuts to isolate the elastic channel. Events from H and D will be distinguished through a multi-parameter fit to the missing mass and energy distributions. Fermi broadening in the deuteron generates peaks that are typically twice as wide as for hydrogen, for the conditions of this proposal. Due to this mixing, the errors will be approximately 1.4 times bigger than for targets which contain only H or D plus heavy materials such as nitrogen or aluminum.

The beam polarization will be measured periodically with the standard Hall-B Moller polarimeter.

#### 4.1.4 The Impact of Møller Scattering

One of the main sources of background produced by a high-energy electron beam impinging upon a HD target is due to interactions of the electron beam with the atomic electrons (Møller scattering). This rate is several orders of magnitude larger than the inelastic hadronic production rate. A dedicated Monte Carlo study aimed to evaluate the impact of the Møller scattering on the detector occupancies has been performed using the CLAS12 GEANT4 based MC (gemc). The CLAS12 response to a single SIDIS event in gemc is shown in Fig. 15.

The effect of the target field on Møller electrons is shown in Fig. 16. The CLAS12 DC occupancies with the HD-Ice transverse magnet energized and a luminosity of  $10^{34}\text{cm}^{-2}\text{sec}^{-1}$ , which is the goal of the proposed experiment, are comparable (slightly below) with the nominal CLAS12 configuration, see Fig. 17.

## 4.2 The CLAS12 Particle Identification

The proposed experiment will use the upgraded CLAS12 spectrometer with the low threshold Cherenkov counter replaced by a RICH detector.

In the baseline design of CLAS12, particle identification (PID) in the forward detector is obtained by using the high threshold Cerenkov counter (HTCC), the low threshold Cerenkov counter (LTCC) and the Time-of-flight scintillator arrays (TOF) (see Fig. 18). In the  $\sim 2.5 - 5 \text{ GeV}/c$  momentum region, the  $\pi/K$  separation relies only on the LTCC performance. Moreover, in the  $4.7 - 8 \text{ GeV}/c$  momentum region it is not possible to separate protons from kaons. In general, this PID system matches the requirements of the physics program at 12 GeV. However there are some physics reactions of high interest, such as the one covered by this proposal, that cannot be accessed without a better PID, especially for charged kaon detection. At 12 GeV for semi-inclusive processes, the  $K/\pi$  ratio is of the order of 10 – 15% (see Fig. 19) thus the required rejection factor for pions is around 1 : 1000 (corresponding to  $4.7\sigma$



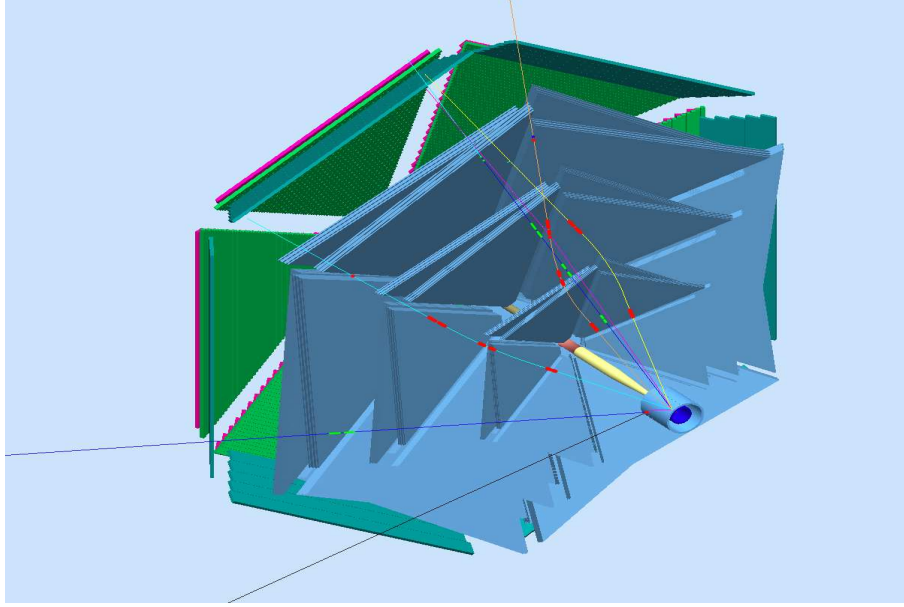


Figure 15: A single SIDIS event in CLAS12 from gemc.

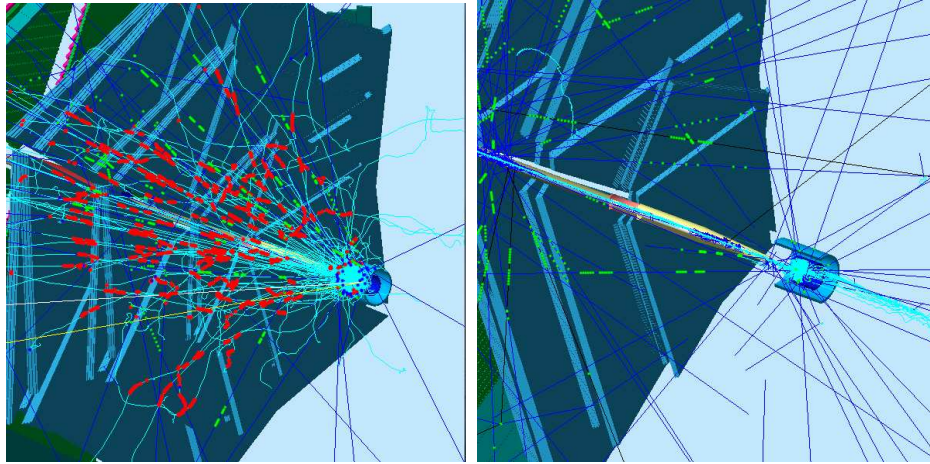


Figure 16: Comparison of the CLAS12 response without (left) and with (right) the target transverse field with the compensation coil. The blue lines are photons, the cyan are electrons.

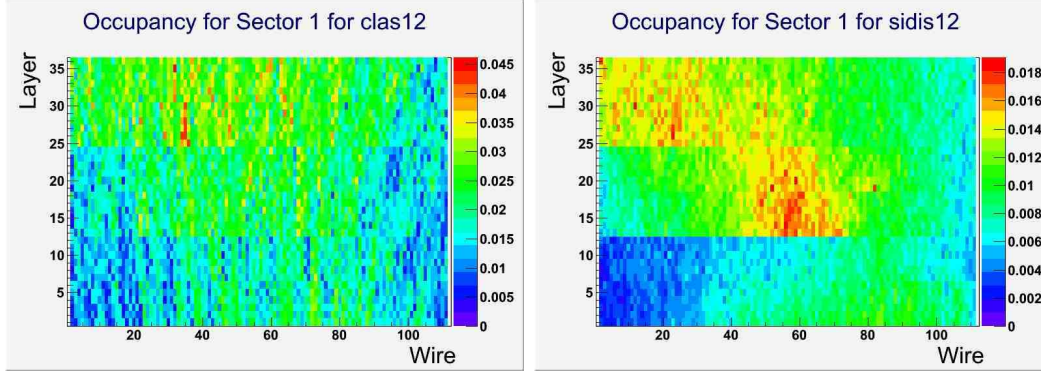


Figure 17: Comparison of the CLAS12 DC occupancies for the regular solenoid field at  $10^{35}\text{cm}^{-2}\text{sec}^{-1}$  (left) and the HD-Ice transverse magnet at  $10^{34}\text{cm}^{-2}\text{sec}^{-1}$  (right).

pion-kaon separation) while with the present configuration, assuming a pion detection inefficiency for the LTCC of 10%, the  $\pi/K$  contamination is 1 : 1. A RICH detector, to be installed in place of the low threshold Cerenkov counter, will significantly improve the CLAS12 particle identification overcoming the above limitations without having any impact on the baseline design of CLAS12.

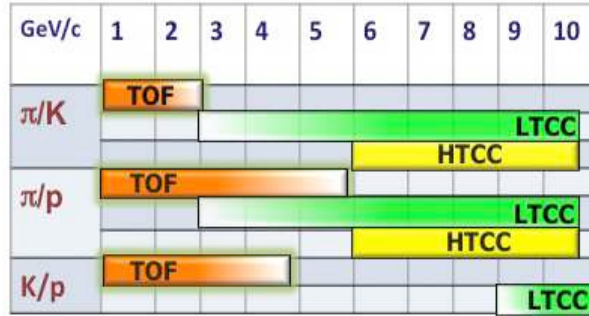


Figure 18: Hadron particle identification in CLAS12.

### 4.3 The CLAS12 RICH detector

To fit the CLAS12 geometry, the RICH should have a projective geometry with six sectors matching the torus bores and covering scattering angles from  $3^\circ$  to  $30^\circ$  (see Fig. 20). Being downstream to the torus magnet at more than 5 m from the interaction point, the RICH has to cover a large surface, each sector having an area of the order of  $4\text{ m}^2$  in the front and  $8\text{ m}^2$  in the back. The RICH depth cannot exceed 1 m, being the detector constrained between existing equipments; the proposed

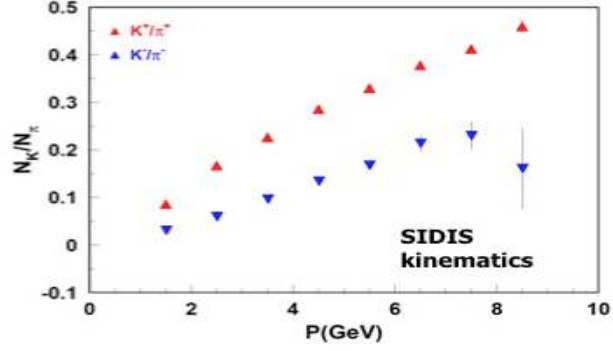


Figure 19: Semi-Inclusive kaon versus pion yield ratio.

solution is based on the concept of the proximity focusing RICH, with mirrors mainly devoted to reduce the photon detector area. In the momentum range of interest an aerogel RICH represents the best solution for the identification of  $\pi/K/p$  as shown in Fig. 21. This implies detecting Cherenkov light in the visible wavelength range and using photomultipliers (PMTs) as photon detectors. On going Monte Carlo studies (see next section) show that a pion-kaon separation greater than  $4\sigma$  at  $8\text{ GeV}/c$  momentum can be achieved if the detector pad size is less than  $1 \times 1\text{ cm}^2$ , thus the use of Multi-Anode PMTs is mandatory.

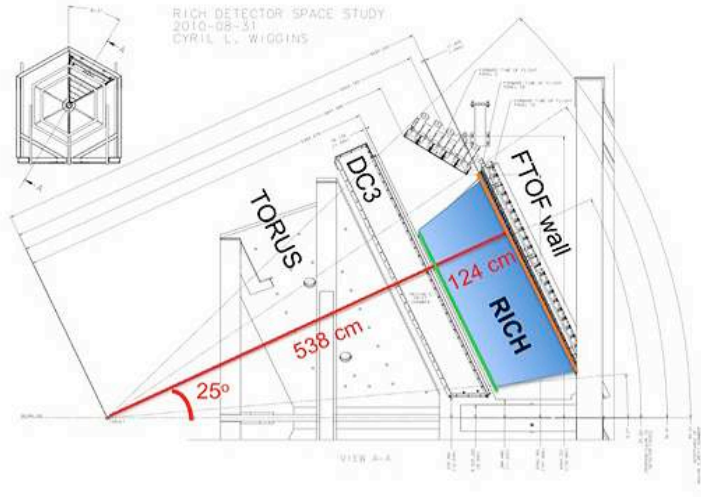


Figure 20: RICH detector space and position in the CLAS12 spectrometer.

The use of aerogel as radiator and the detection of light in the visible wavelength range is an expensive solution. Work is in progress to limit the area of the pho-

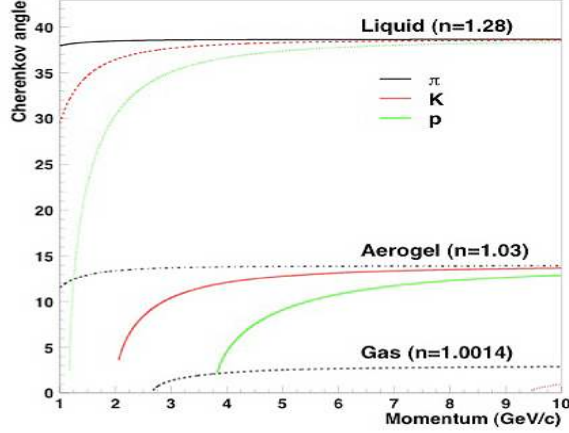


Figure 21: Cherenkov angle versus particle momenta for  $\pi$ ,  $k$ ,  $p$  and different radiators.

ton detector to about  $1m^2$  per sector. The study of the spatial distributions of the Cherenkov photons impact point at the detection surface shows that high-momentum particles concentrate in a limited forward region close to the beam line (see Fig. 22).

The approach is, thus, to instrument a limited area around the beam line to have direct detection in the forward region at high momenta, while at large angles and lower momenta a system of focusing mirrors catches the light and reflect it toward the photon detector. A drawing of the proposed solution is illustrated in Fig. 23 where the main components of the systems are shown: the planar mirror (positioned before the aerogel), the aerogel, the proximity gap, the PMTs plane covering the angular region between  $3^\circ$  and  $14^\circ$ , and the elliptical mirror which reflects the light produced by the particles emitted at angles larger than  $14^\circ$  towards the planar mirror.

#### 4.3.1 Preliminary Monte Carlo results

Preliminary Monte Carlo studies based on GEANT4 with a realistic geometry of the CLAS12 detector and events generated with Pythia have been performed with the aim to optimize all the component of the detector. The dimensions of the radiator thickness and the gap length as well as the pad/pixel size of the photon detector have been varied in order to find the optimal combination which gives the smallest reconstruction error in the Cerenkov angle and the highest number of photoelectrons. An average number of 10 and 5 photoelectrons has been obtained for the direct and reflected light collection, respectively. An example of simulated events in the proposed RICH geometry is shown in Fig. 24 where Cherenkov light direct detected and detected after the elliptical mirror reflection is clearly visible.

In order to have a precise information about the RICH performances in terms of pion/kaon separation a pattern recognition algorithm based on the event-wise Direct Ray Tracing (DRT) technique has been implemented; DRT combines the track(s)

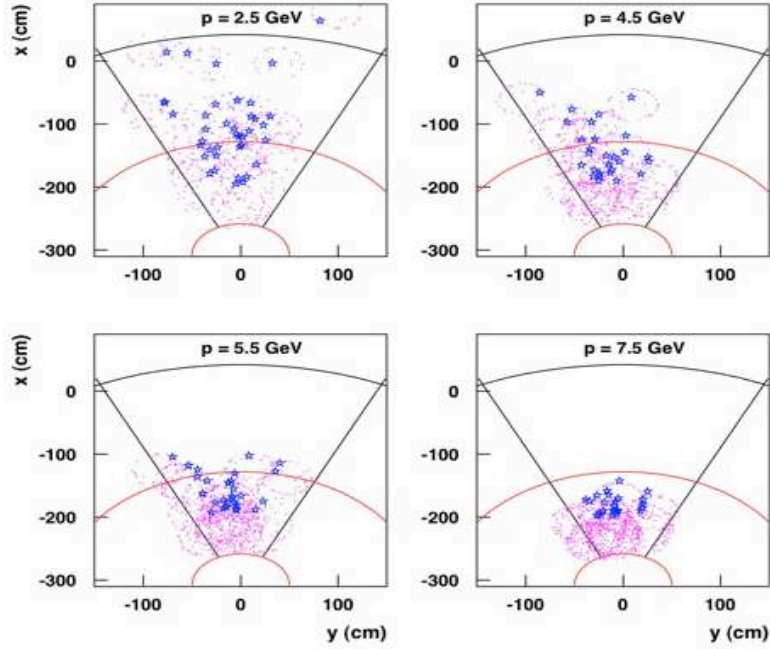


Figure 22: Spatial distributions of the particle impact point at the RICH entrance (stars) and gamma impact point at the detector surface (dots) for few overlapped events. The plots distinguish among particle of increasing average momentum, from  $2.5 \text{ GeV}/c$  up to  $7.5 \text{ GeV}/c$ , from top to bottom and left to right. High-momentum particles concentrate in a limited forward region close to the beam line, arbitrarily delimited by the two dashed lines just for an illustration porpouse.

information with all feasible hypotheses on the tracking particle(s) and realistically estimates, for each hypothesis, the produced photon hits patters, which are combined to the simulated/measured one by means of a likelihood function. The most probable particle(s) hypothesis is assumed as the true one. The results obtained using the RICH configuration shown in Fig. 23 with aerogel of increasing thickness from 2 to 6 cm, a gap length of  $\sim 100 \text{ cm}$  and a pad size of  $0.6 \text{ cm}$  and for particle momenta in the range  $7\text{-}9 \text{ GeV}/c$  is shown in Fig. 25. In the figure the likelihood for the different particles hypothesis is shown. As it can be seen the contamination is widely smaller than 1%. For instance, the probability that a pion is misidentified as a kaon is 0.18% which corresponds to approximatively a  $4\text{-}5 \sigma$  pion/kaon separation.

The preliminary results of the ongoing Monte Carlo analysis are ecouraging about the performances of the proposed RICH; several potential improvements have been already identified and are under detailed investigation. Also test in realistic conditions of the proposed solution with a small prototype is underway.



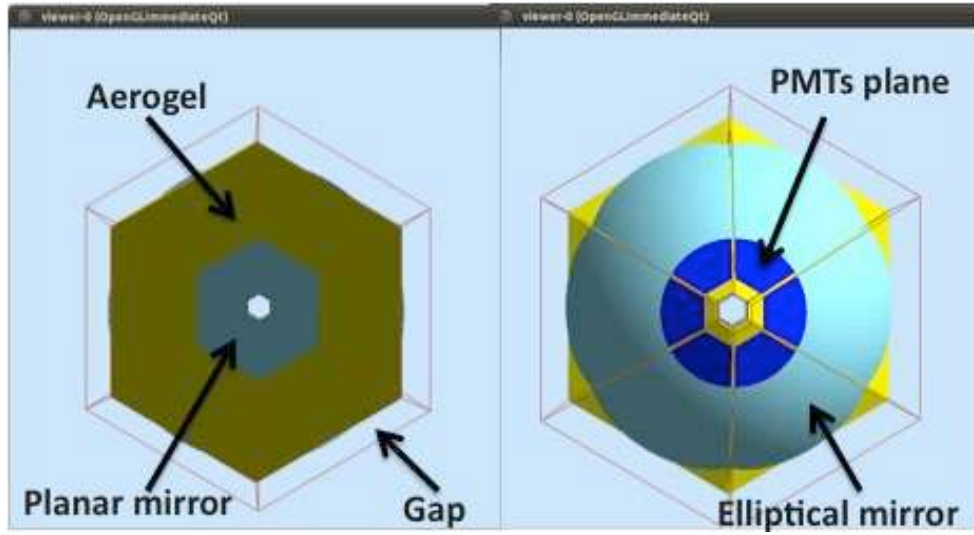


Figure 23: Drawing of the proposed proximity focusing RICH with focusing mirrors.

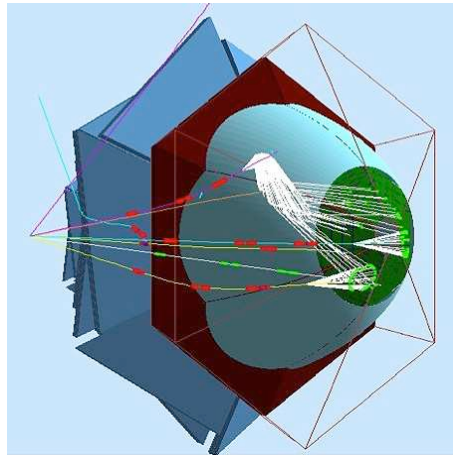


Figure 24: Exemple of events simulated with GEANT4

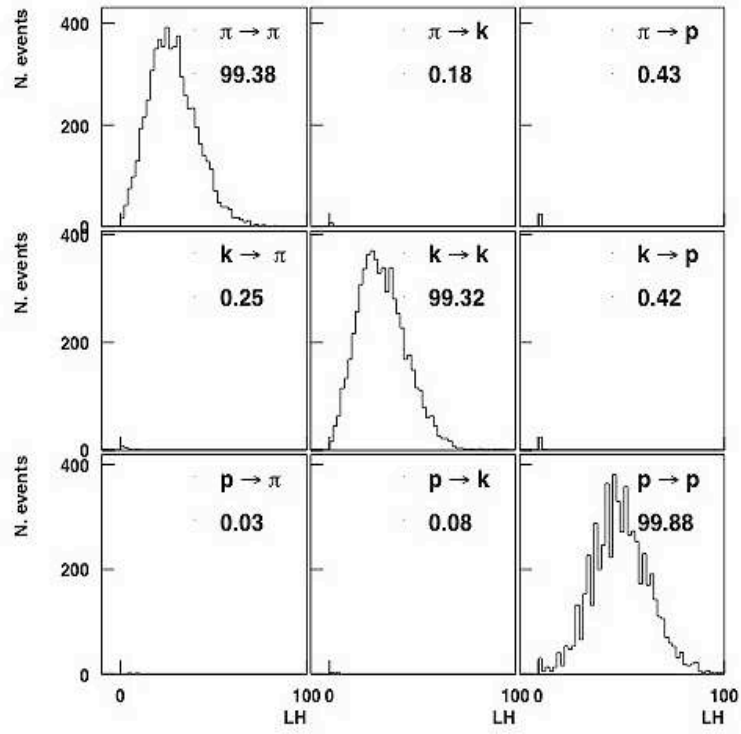


Figure 25: Likelihood distribution for the different particles hypothesis.

## 4.4 The Measurement

### 4.4.1 Event Identification, Reconstruction, and Acceptances

Final-state hadrons and the scattered electron will be detected by the CLAS12 spectrometer. Electrons are separated from heavier particles using Cherenkov counters and electromagnetic calorimeters. Pions will be identified using Cherenkov counters and measurement of time of flight. The use of the CLAS12 RICH detector would ensure pion/kaon separation in a wide momentum range (up to approximately  $8 \text{ GeV}/c$ ). Pion and kaon momenta will be reconstructed in the CLAS12 drift chamber system, embedded within the toroidal magnetic field. For the proposed experiment, photons from  $\pi^0$  decays (or from  $\eta$  decays) will be reconstructed using the forward angle electromagnetic calorimeter (FC) and the new preshower calorimeter (PCAL). Kinematical distributions of electrons and final state hadrons are shown in Fig. 26 and Fig. 27.

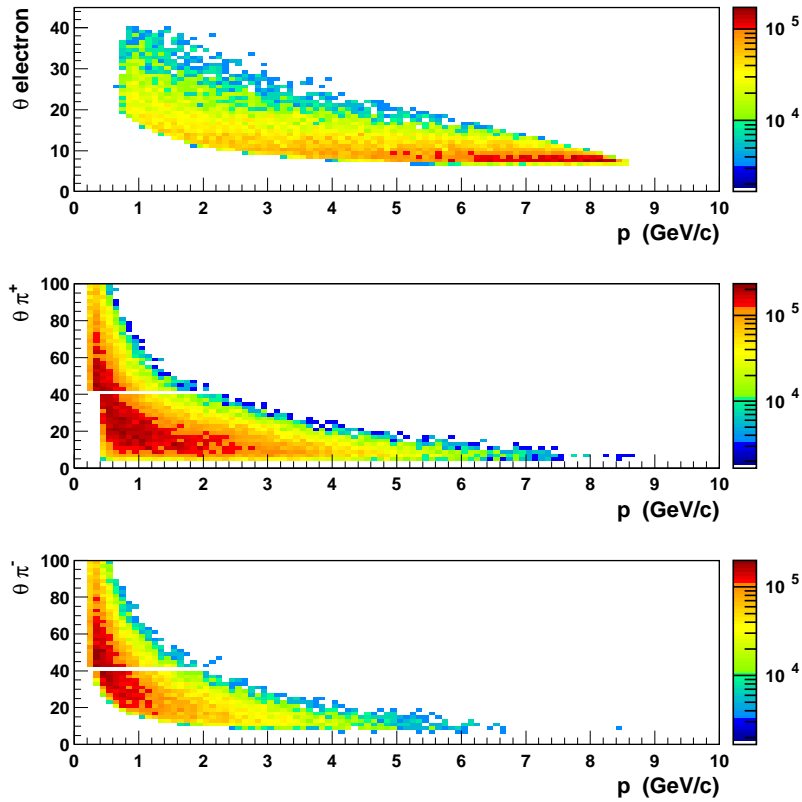


Figure 26: Kinematical distributions of electrons and final state hadrons.



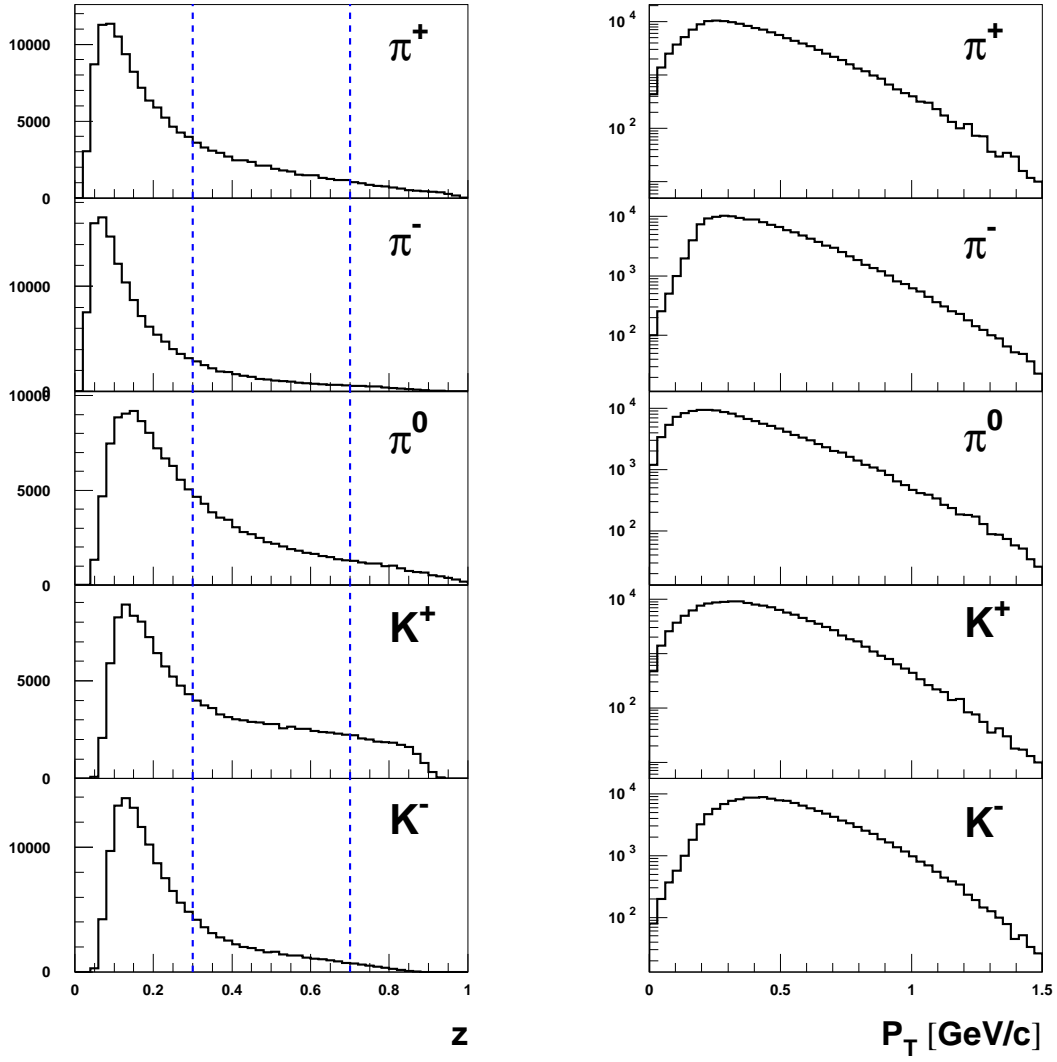


Figure 27: Typical kinematic distributions of CLAS12 SIDIS hadrons with transverse target. The dashed lines define the  $z$  region selected for SIDIS.

Fig. 28 shows the correlation of relevant kinematical variables with the scattering angle. Electron detection at large angles (larger than 20 degrees) is mandatory to explore the large  $Q^2$  regime, whereas hadron identification is required in the middle angle range (15-20 degrees) to reach large  $P_T$  values. The CLAS12 forward detector is perfectly suitable for such measurements since designed to cover up to 40 degrees angles.

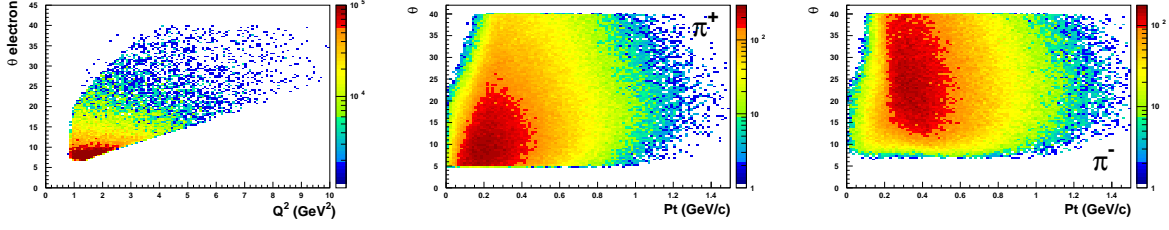


Figure 28: Kinematic coverage of CLAS12 SIDIS hadrons with transverse target.

#### 4.4.2 Acceptance and Data Analysis

Although SSAs typically are not too sensitive to acceptance corrections, in the case of the transverse target, due to the large number of contributions appearing as different azimuthal moments in the cross section, the acceptance corrections are more important. The analysis of the transverse target requires fits in the 2-dimensional space of the relevant azimuthal angles  $\phi$  and  $\phi_S$ . A detailed procedure on the accounting for acceptance corrections in the separation of the different azimuthal moments was developed by the HERMES collaboration. According to this method, the evaluation of the acceptance effects on the measured asymmetry amplitudes is achieved through the difference between a fully-differential (thus free from acceptance effects) parametrization of the extracted asymmetries, and the asymmetries extracted from a Monte Carlo simulation which accounts for the full geometry of the detector (i.e. including the detector acceptance and smearing). A similar procedure will be applied to estimate the expected acceptance corrections for e.g. the Sivers and Collins asymmetries, extracted in the CLAS12 acceptance.

#### 4.4.3 Count Rates and Statistical Errors

The expected number of counts is given by

$$N = \mathcal{L} \times \text{time} \times \sigma \times (\Delta Q^2 \cdot \Delta x_B) \times \Delta z \times \Delta P_T \times \Delta \phi \times (\Delta \varphi_e)_{\text{eff}} / 2\pi . \quad (15)$$

With the proposed configuration as described in Section 4.1, a luminosity of  $10^{34} \text{ cm}^{-2}\text{s}^{-1}$  is expected. The yields of SIDIS pions and kaons for the proposed experiment

is calculated for 80 days of measurements (i.e. for the total requested beam time, 100 days, diminished by a 20% duty-factor accounting for calibration runs, empty target runs, and supportive tests). The expected number of SIDIS pions and kaons within the kinematic limits:  $Q^2 > 1 \text{ GeV}^2$  (corresponding to  $x > 0.05$ ),  $W^2 > 4 \text{ GeV}^2$ ,  $0.10 < y < 0.85$  and  $0.3 < z < 0.7$  are:  $27.5 \cdot 10^6$ ,  $9.1 \cdot 10^6$  and  $7.8 \cdot 10^6$  for  $\pi^+$ ,  $\pi^-$ , and  $\pi^0$ , respectively, and  $2.9 \cdot 10^6$  and  $0.6 \cdot 10^6$  for  $K^+$  and  $K^-$ , respectively. A squared missing mass greater than  $2 \text{ GeV}^2$  was required to suppress contamination from exclusive channels. In particular, the  $\pi^0$  yields were obtained selecting the range  $0.097 < m_{\gamma\gamma} < 0.179 \text{ GeV}/c^2$  of the  $2\gamma$  invariant mass spectrum, corresponding to  $\pm 2\sigma$  from the mean value ( $\langle m_{\gamma\gamma} \rangle = 0.138 \text{ GeV}/c^2$ ).

The hydrogen target polarization is assumed to be 75%, whereas a beam polarization of 85% is predicted. The dilution factor for the hydrogen target is of the order of 1/3. All the above factors have been taken into account when calculating the statistical uncertainties on the asymmetries (see Section 4.5). The number of days was chosen to achieve a statistical error that is not significantly larger than the systematical error at the highest  $x$  and  $P_T$  points.

#### 4.4.4 Systematic Errors

The systematic uncertainties can be divided into two categories: those that scale with the measured asymmetry and those that are independent of the measured results. In the first category, the dominant uncertainty is expected to be that from the target polarization and the dilution from the unwanted HD and Al backgrounds. For the second category, we have taken our best estimate of the magnitude of the systematic effect, and divided by the average expected proton asymmetry.

One of the main contributions to the estimated relative uncertainties, summarized in Table 7, comes from the procedure used to separate the azimuthal moments of interest from other, potentially non-zero, azimuthal asymmetries (for example a twist-3  $\sin(\phi_S)$  moment). Another large contribution is from possible contamination of the SIDIS pion event sample by pions from decays of diffractive vector mesons, mainly  $\rho^0$  (the contamination for kaons is expected to be much smaller). Thanks to the large acceptance of CLAS12, the asymmetries from background processes, such as  $\rho^0$  production, will be measured simultaneously and can thus be corrected for, as the size of the contamination can be measured as well. Based on our previous studies for the EG1, e1f and e16 experiments, the uncertainty from radiative corrections will be negligible.

We conservatively estimate the average total relative systematic error on the proton SSAs to be of order 10%, sufficiently small for a very significant measurement.

Error source	Systematic error (%)
H/D background	4
Target polarization $P_T$	4
acceptance corrections	4
Al background contribution	3
$\rho^0$ contamination	3
Radiative corrections	2
Total	$\sim 8$

Table 5: Estimated contributions to the relative systematic uncertainty on the proton TTSA's in SIDIS.

## 4.5 Projected Results

The projected CLAS12 statistical precision for Collins and Sivers amplitudes corresponding to 80 days of data-taking with the HD-Ice target are shown for pions and charged kaons as a function of  $x$  in Figs. 29-30. The kinematic region considered for these projections is the following:  $Q^2 > 1 \text{ GeV}^2$  (corresponding to  $x > 0.05$ ),  $W^2 > 4 \text{ GeV}^2$ ,  $0.10 < y < 0.85$  and  $0.3 < z < 0.7$ . A squared missing mass greater than  $2 \text{ GeV}^2$  was also required. In particular, the  $\pi^0$  yields were obtained selecting the range  $0.097 < m_{\gamma\gamma} < 0.179 \text{ GeV}/c^2$  of the  $2\gamma$  invariant mass spectrum, corresponding to  $\pm 2\sigma$  from the mean value ( $\langle m_{\gamma\gamma} \rangle = 0.138 \text{ GeV}/c^2$ ). The projected results were obtained from a Monte Carlo simulation including a description of the CLAS12 geometry as well as detector acceptance and smearing effects. QED radiative effects were neglected since known, from previous studies, to be negligibly small. Here, a target polarization of 75% and a dilution factor of 1/3 were assumed.

In most of the cases the CLAS12 error bars (statistical uncertainties) are not visible since they are smaller than the dots symbols. The comparison between the projected results for CLAS12 and the HERMES results (Fig. 29-30) shows the remarkable improvement expected for CLAS12 in terms of statistical precision and kinematic coverage, especially in the valence region (intermediate-to-high  $x$ ).

In Figs. 31-32, projected results are shown as a function of  $x$  for 2-dimensional extractions of the Sivers amplitudes in bins of  $P_T$  and  $z$ , respectively. The Sivers effects was implemented in the Monte Carlo generator using a fully-differential model tuned to HERMES data and evaluated event-by-event at the CLAS12 kinematics. The projected results show sizable Sivers amplitudes for  $\pi^+$  and  $\pi^0$ . However, the magnitude of the projected amplitudes for CLAS12 is purely indicative, as it results from an extrapolation of the HERMES model into the CLAS12 kinematic region.

The measurement of the transverse asymmetry from the Sivers effect with  $\pi^0$  will provide a model-independent extraction of the Sivers function in the large- $x$  region, where the sea contribution is not significant. Furthermore, measurements of amplitudes for identified pions and kaons will provide precious information not only on the contribution to the distribution functions involved from the various quark flavors (e.g., it would allow for constraints on the contribution from the strange sea quarks), but also on the ratio of favored to unfavored polarized fragmentation functions, complementary to  $e^+e^-$  data.

Thanks to the high statistics achievable in 80 days of measurements, a 4-dimensional analysis of the extracted azimuthal moments can be performed. This allows the disentanglement of all the specific kinematical dependences and a deeper inspection of the mechanisms generating the asymmetries. For example, the  $Q^2$  dependence can constrain the higher-twist contributions, whereas the  $P_T$  dependence links to the perturbative to non-perturbative transition. The projected statistical precision for a 4-dimensional analysis of the Sivers amplitudes are reported for  $\pi^+$  and  $K^+$  in Figs. 33-34. In the proposed data-taking time, a precise mapping of a large portion of the phase-space is achievable for pions, extending into the high- $Q^2$  high- $P_{h\perp}$  region

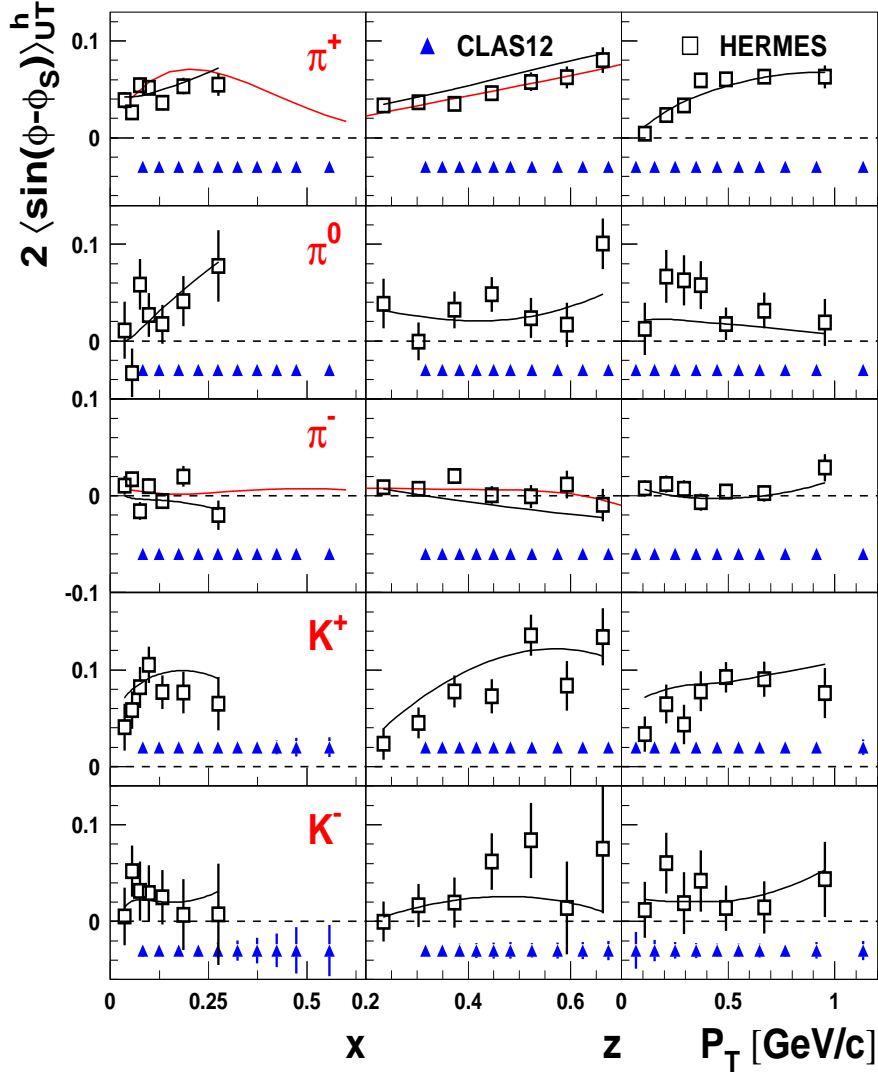


Figure 29: Expected statistical uncertainty for the Sivers amplitudes as a function of  $x$ ,  $z$  and  $P_T$ . Overlaid are also shown the corresponding HERMES results. The curves show the predictions from a 4D parameterization extracted from the HERMES data (black line) and a phenomenological model (red line).

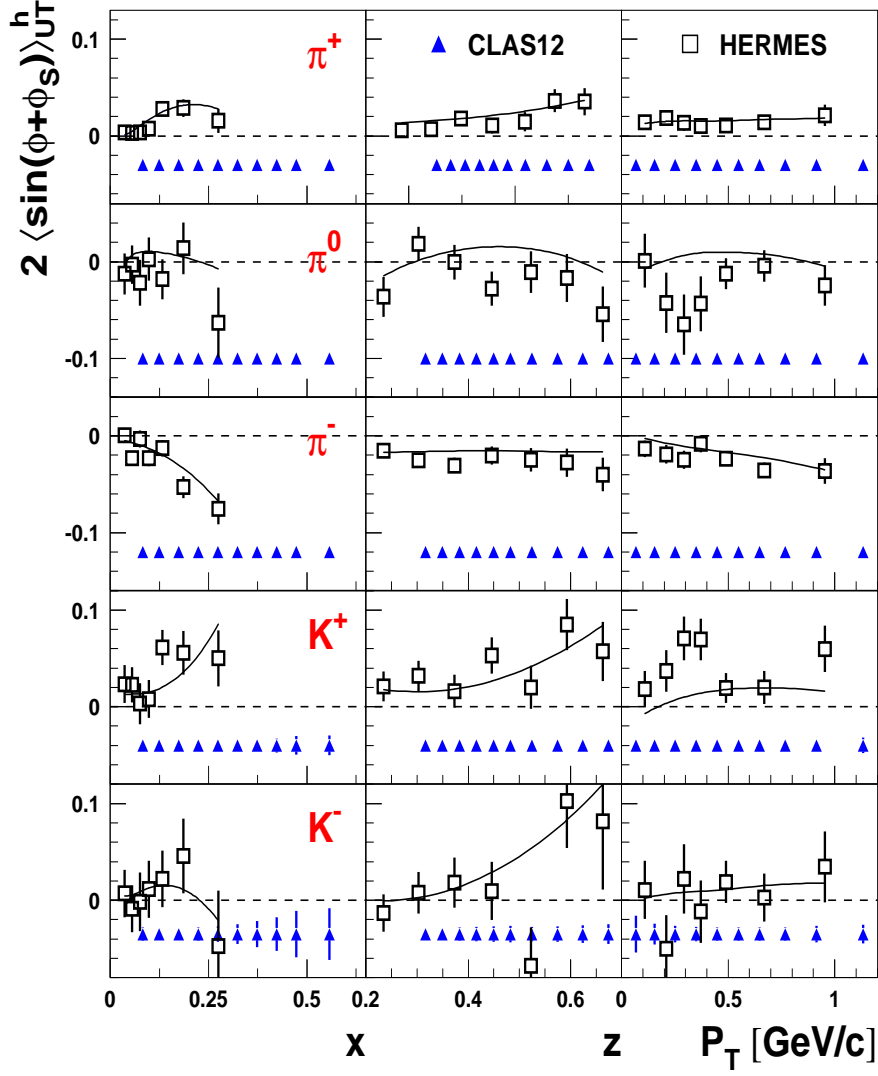


Figure 30: Expected statistical uncertainty for the Collins amplitudes as a function of  $x$ ,  $z$  and  $P_T$ . Overlaid are also shown the corresponding HERMES results. The curves show the predictions from a 4D parameterization extracted from the HERMES data.

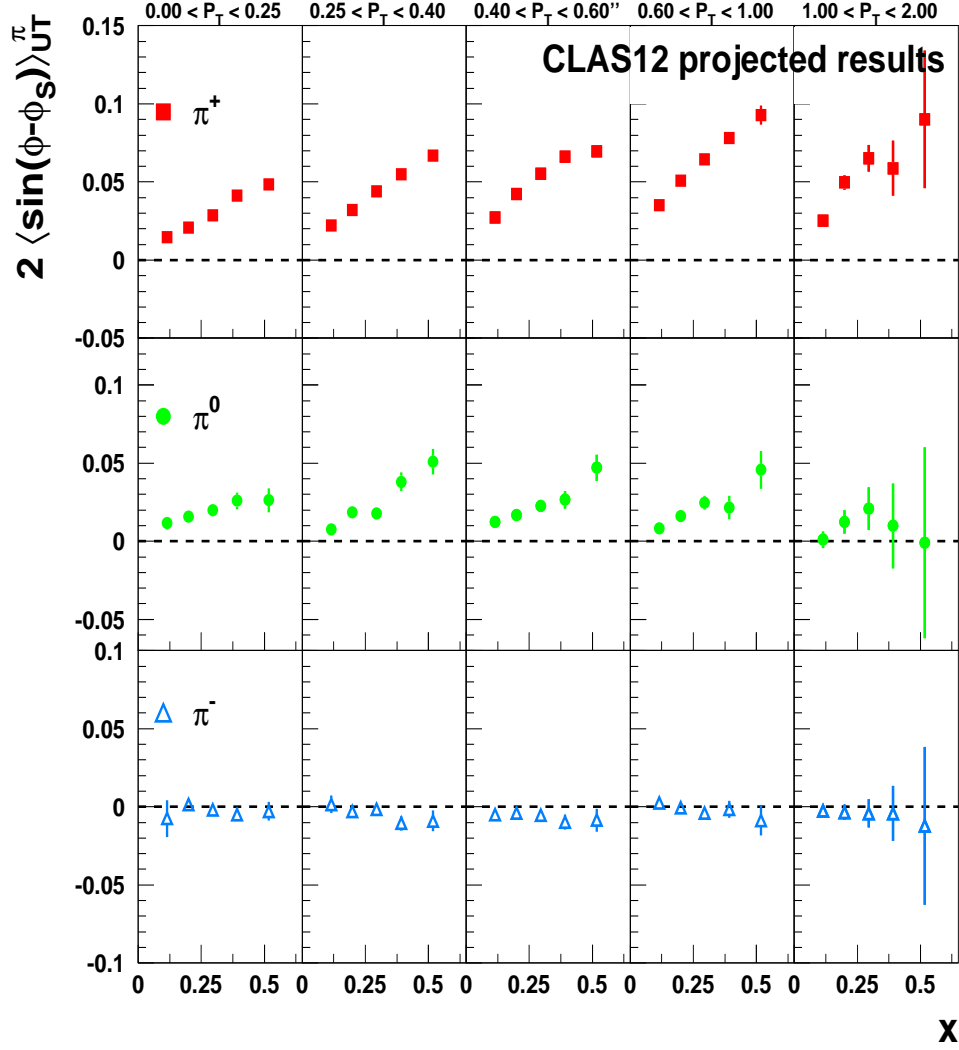


Figure 31: Expected 2-dimensional projections for the Sivers amplitudes (based on a 4D parameterization extracted from the HERMES data). Bins in  $P_T$  as a function of  $x$  for  $\pi^+$  (top row),  $\pi^0$  (middle row) and  $\pi^-$  (bottom row).



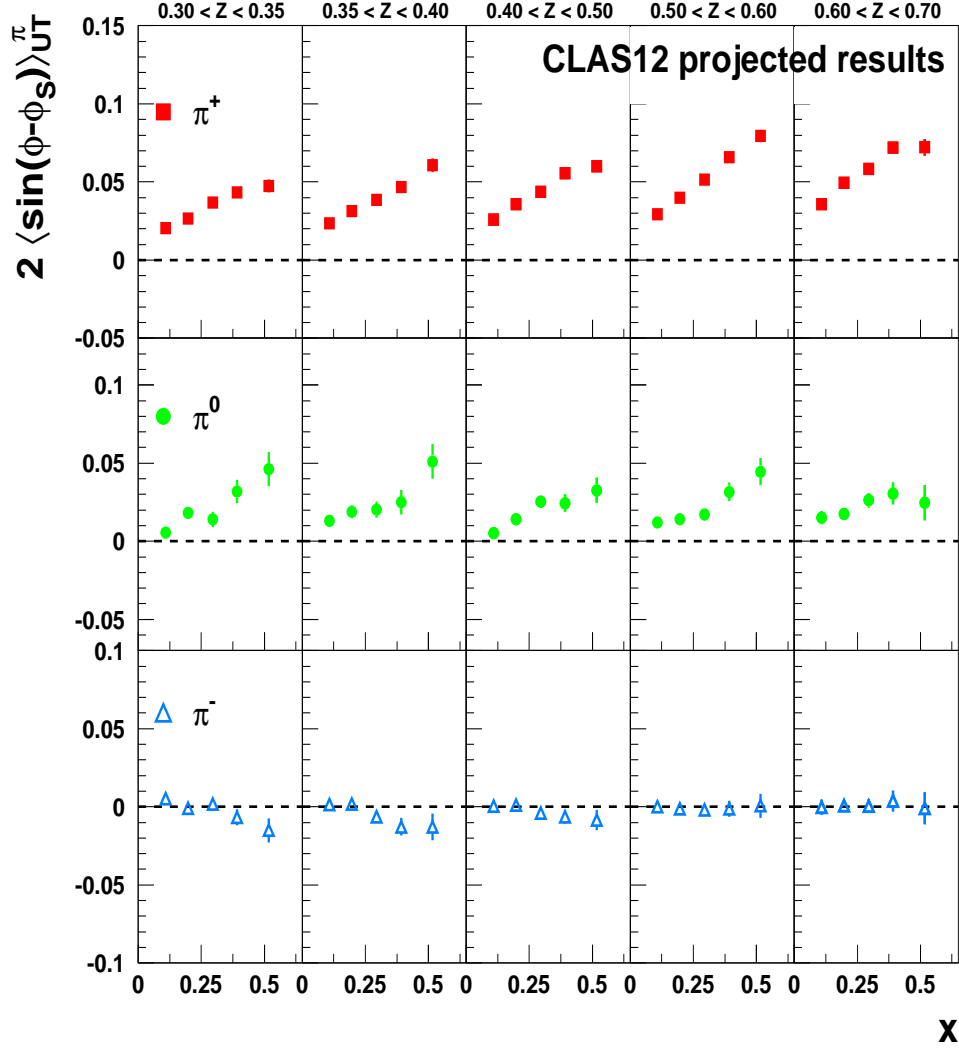


Figure 32: Expected 2-dimensional projections for the Sivers amplitudes (based on a 4D parameterization extracted from the HERMES data). Bins in  $z$  as a function of  $x$  for  $\pi^+$  (top row),  $\pi^0$  (middle row) and  $\pi^-$  (bottom row).

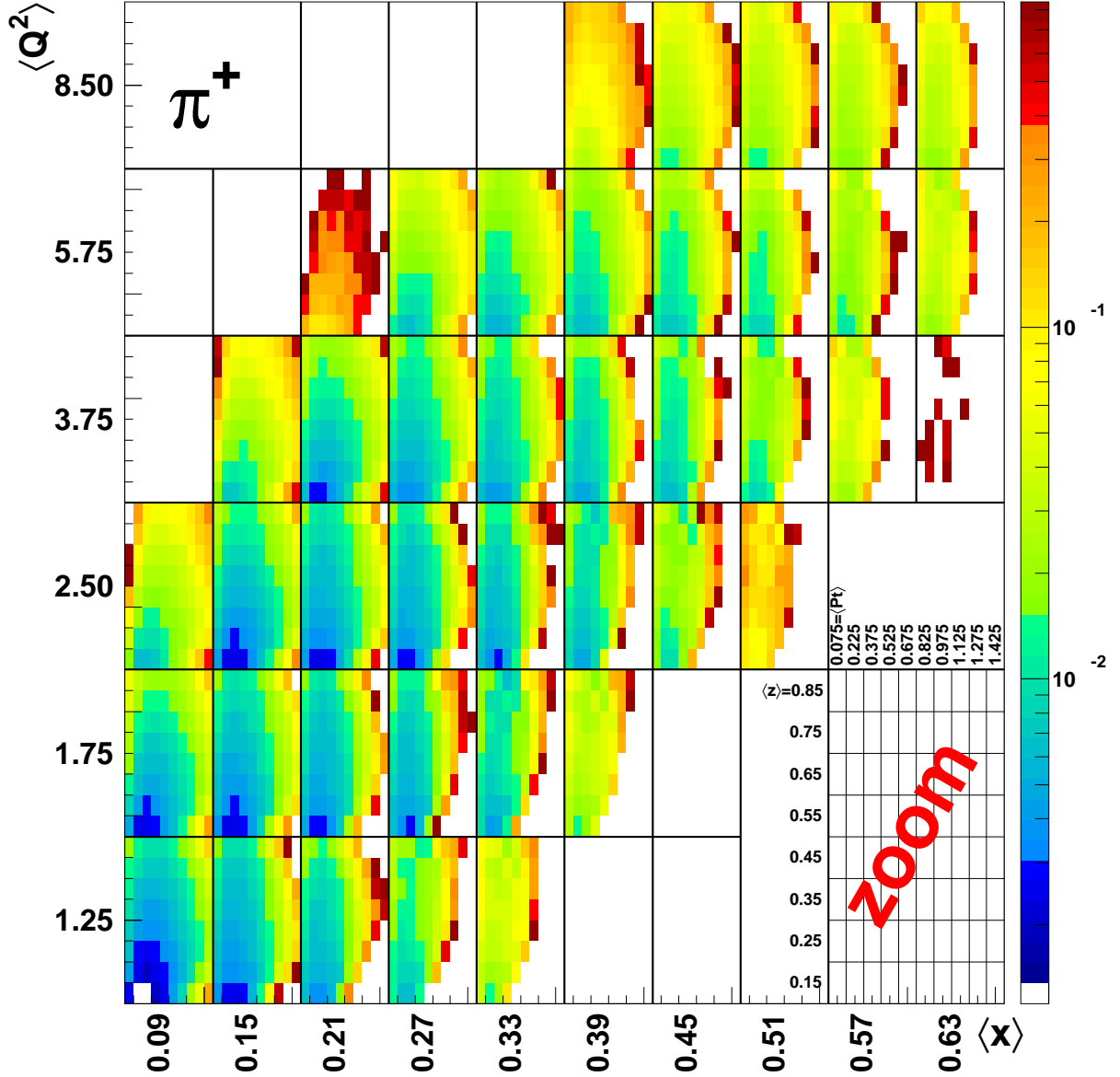


Figure 33: Expected statistical error in a 4-dimensional analysis of the Siverts TTSA  $A_{UT}^{\sin(\phi-\phi_S)}$  for  $\pi^+$ . Each  $x$ - $Q^2$  bin is subdivided in a matrix of  $z$ - $P_{h\perp}$  bins, as depicted in the insert (zoom). For each bin the average kinematical values are reported. The color corresponds to the statistical error that can be achieved in 80 days of data-taking. Note a precision of few percents can be obtained even in the high- $Q^2$  bins for  $P_T$  values up to 1 GeV/c.

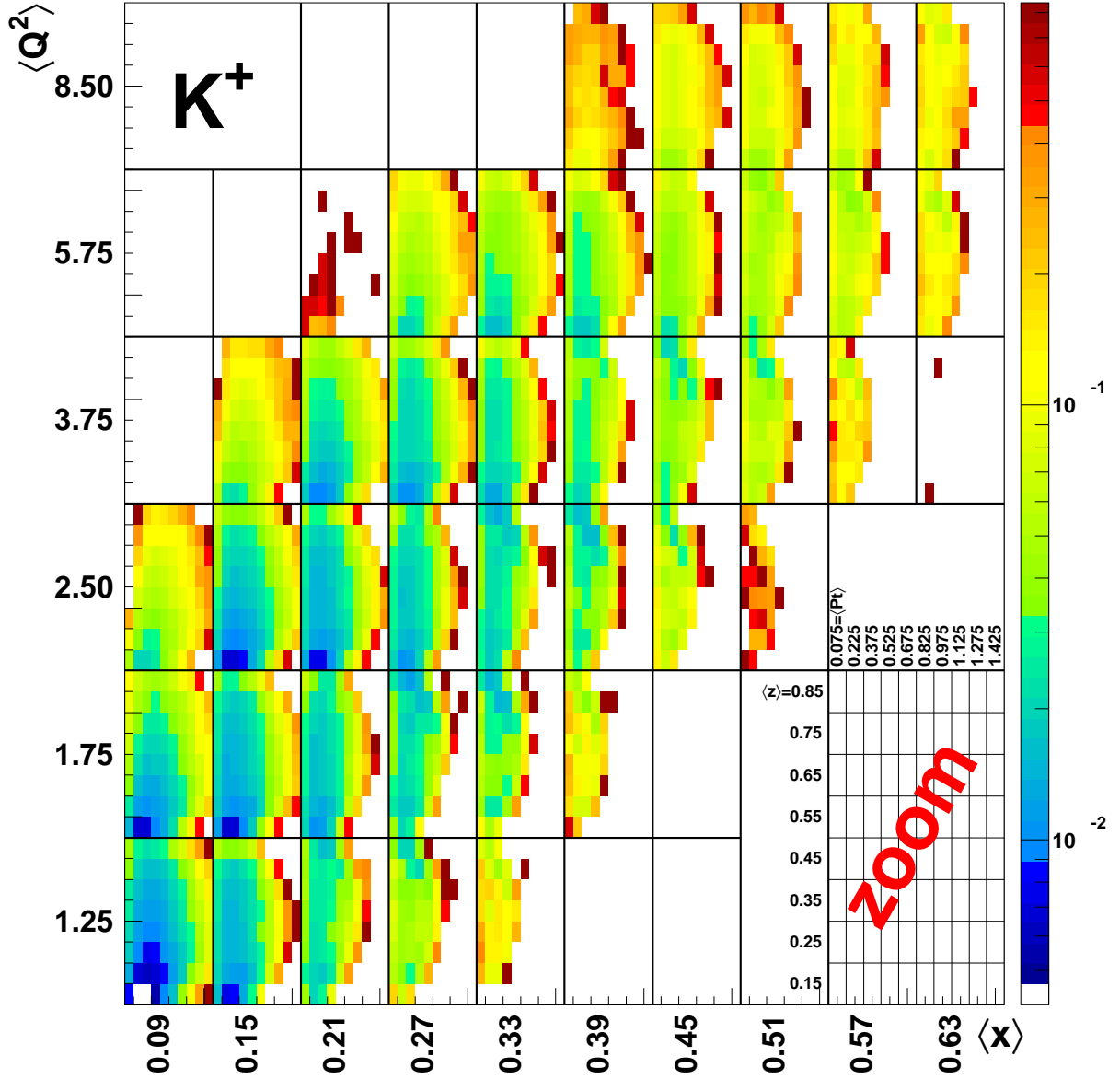


Figure 34: Expected statistical error in a 4-dimensional analysis of the Siverts TTSA  $A_{UT}^{\sin(\phi-\phi_S)}$  for  $K^-$ . Each  $x$ - $Q^2$  bin is subdivided in a matrix of  $z$ - $P_{h\perp}$  bins, as depicted in the insert (zoom). For each bin the average kinematical values are reported. The color corresponds to the statistical error that can be achieved in 80 days of data-taking. Note a precision of few percents can be obtained in a large portion of the phase space.

of interest. In particular a precision of few percents can be obtained at large  $Q^2$  for values of  $\mathbf{P}_{h\perp}$  up to 1 GeV/c. An extended mapping is possible also in the kaon sector, although with a precision limited by the smaller yields.

## 4.6 Fourier Transformed Cross Sections

TMDs and transverse momentum-dependent fragmentation functions enter the SIDIS cross section in a convolution with respect to transverse momentum. In order to extract TMDs, it is therefore advantageous to project the differential cross section onto Fourier modes [118]. The result is a product of TMDs and fragmentation functions in Fourier space. The Fourier transform of a generic TMD  $f$  and a generic fragmentation function  $D$  is defined as

$$\tilde{f}(x, \mathbf{b}_T^2) \equiv \int d^2 \mathbf{k}_T e^{i \mathbf{b}_T \cdot \mathbf{k}_T} f(x, \mathbf{k}_T^2) = 2\pi \int d|\mathbf{k}_T| |\mathbf{k}_T| J_0(|\mathbf{b}_T| |\mathbf{k}_T|) f^a(x, \mathbf{k}_T^2), \quad (16)$$

$$\tilde{D}(z, \mathbf{b}_T^2) \equiv \int d^2 \mathbf{p}_T e^{i \mathbf{b}_T \cdot \mathbf{p}_T} D(z, \mathbf{p}_T^2) = 2\pi \int d|\mathbf{p}_T| |\mathbf{p}_T| J_0(|\mathbf{b}_T| |\mathbf{p}_T|) D^a(z, \mathbf{p}_T^2), \quad (17)$$

where  $J_0$  is a Bessel function. We also need to introduce  $\mathbf{b}_T^2$ -derivatives of the Fourier transformed distributions:

$$\begin{aligned} \tilde{f}^{(n)}(x, \mathbf{b}_T^2) &\equiv n! \left( -\frac{2}{M^2} \partial_{\mathbf{b}_T^2} \right)^n \tilde{f} = \frac{2\pi n!}{(M^2)^n} \int d|\mathbf{k}_T| |\mathbf{k}_T| \left( \frac{|\mathbf{k}_T|}{|\mathbf{b}_T|} \right)^n J_n(|\mathbf{b}_T| |\mathbf{k}_T|) f(x, \mathbf{k}_T^2), \\ \tilde{D}^{(n)}(z, \mathbf{b}_T^2) &\equiv n! \left( -\frac{2}{z^2 M_h^2} \partial_{\mathbf{b}_T^2} \right)^n \tilde{D} = \frac{2\pi n!}{(z^2 M_h^2)^n} \int d|\mathbf{p}_T| |\mathbf{p}_T| \left( \frac{|\mathbf{p}_T|}{|\mathbf{b}_T|} \right)^n J_n(|\mathbf{b}_T| |\mathbf{p}_T|) D(z, \mathbf{p}_T^2). \end{aligned} \quad (18)$$

With these definitions, we can identify the Fourier-modes of the cross section as products of the  $\tilde{f}^{(n)}$  and  $\tilde{D}^{(n)}$ . At leading twist and tree-level, we find in the  $\phi_h$ -independent channel

$$\begin{aligned} &\int_0^{2\pi} \frac{d\phi_S}{2\pi} \int_0^{2\pi} d\phi_h \int_0^\infty d|\mathbf{P}_{h\perp}| |\mathbf{P}_{h\perp}| J_0(|\mathbf{P}_{h\perp}| |\mathbf{b}_T|) \left[ \frac{d\sigma}{dx_B dy d\phi_S dz_h d\phi_h |\mathbf{P}_{h\perp}| d|\mathbf{P}_{h\perp}|} \right] \\ &= \frac{\alpha^2}{y Q^2} \frac{y^2}{(1-\varepsilon)} \left( 1 + \frac{\gamma^2}{2x_B} \right) \sum_a e_a^2 \left\{ \tilde{f}_1^{a(0)}(x, z^2 \mathbf{b}_T^2) + S_{\parallel} \lambda_e \sqrt{1-\varepsilon^2} \tilde{g}_1^{(0)a}(x, z^2 \mathbf{b}_T^2) \right\} \tilde{D}_1^{(0)a}(z, \mathbf{b}_T^2), \end{aligned}$$

where  $e_a$  is the electric charge of a quark of flavor  $a$ . The unpolarized contribution from  $f_1$  can be isolated from that of  $g_1$  by averaging over the helicity of the electron  $\lambda_e$ . The above transformation depends on the external parameter  $\mathcal{B}_T \equiv |\mathbf{b}_T|$ . Choosing different values of this parameter allows us to scan the transverse momentum dependence of the distributions in Fourier space.

A similar integration allows us to project out information on the transversity function  $h_1$ :

$$\begin{aligned} & \int_0^{2\pi} \frac{d\phi_S}{2\pi} \int_0^{2\pi} d\phi_h \sin(\phi_h + \phi_S) \int_0^\infty d|\mathbf{P}_{h\perp}| |\mathbf{P}_{h\perp}| \frac{2J_1(|\mathbf{P}_{h\perp}||\mathbf{b}_T|)}{zM_h|\mathbf{b}_T|} \left[ \frac{d\sigma}{dx_B dy d\phi_S dz_h d\phi_h |\mathbf{P}_{h\perp}| d|\mathbf{P}_{h\perp}|} \right] \\ &= \frac{\alpha^2}{yQ^2} \frac{y^2}{(1-\varepsilon)} \left( 1 + \frac{\gamma^2}{2x_B} \right) |\mathbf{S}_\perp| \varepsilon \sum_a e_a^2 \tilde{h}_1^{(1)a}(x, z^2 \mathbf{b}_T^2) \tilde{H}_1^{\perp(1)a}(z, \mathbf{b}_T^2) . \quad (19) \end{aligned}$$

A similar integration allows us to project out information on the Sivers function  $f_{1T}^\perp$ :

$$\begin{aligned} & \int_0^{2\pi} \frac{d\phi_S}{2\pi} \int_0^{2\pi} d\phi_h \sin(\phi_h - \phi_S) \int_0^\infty d|\mathbf{P}_{h\perp}| |\mathbf{P}_{h\perp}| \frac{-2J_1(|\mathbf{P}_{h\perp}||\mathbf{b}_T|)}{zM|\mathbf{b}_T|} \left[ \frac{d\sigma}{dx_B dy d\phi_S dz_h d\phi_h |\mathbf{P}_{h\perp}| d|\mathbf{P}_{h\perp}|} \right] \\ &= \frac{\alpha^2}{yQ^2} \frac{y^2}{(1-\varepsilon)} \left( 1 + \frac{\gamma^2}{2x_B} \right) |\mathbf{S}_\perp| \sum_a e_a^2 \tilde{f}_{1T}^{\perp(1)a}(x, z^2 \mathbf{b}_T^2) \tilde{D}_1^{(0)a}(z, \mathbf{b}_T^2) . \quad (20) \end{aligned}$$

A similar integration allows us to project out information on the worm gear function  $g_{1T}^\perp$ :

$$\begin{aligned} & \int_0^{2\pi} \frac{d\phi_S}{2\pi} \int_0^{2\pi} d\phi_h \cos(\phi_h - \phi_S) \int_0^\infty d|\mathbf{P}_{h\perp}| |\mathbf{P}_{h\perp}| \frac{2J_1(|\mathbf{P}_{h\perp}||\mathbf{b}_T|)}{zM|\mathbf{b}_T|} \left[ \frac{d\sigma}{dx_B dy d\phi_S dz_h d\phi_h |\mathbf{P}_{h\perp}| d|\mathbf{P}_{h\perp}|} \right] \\ &= \frac{\alpha^2}{yQ^2} \frac{y^2}{(1-\varepsilon)} \left( 1 + \frac{\gamma^2}{2x_B} \right) |\mathbf{S}_\perp| \lambda_e \sqrt{1-\varepsilon^2} \sum_a e_a^2 \tilde{g}_{1T}^{\perp(1)a}(x, z^2 \mathbf{b}_T^2) \tilde{D}_1^{(0)a}(z, \mathbf{b}_T^2) . \quad (21) \end{aligned}$$

A similar integration allows us to project out information on the Pretzelosity function  $h_{1T}^\perp$ :

$$\begin{aligned} & \int_0^{2\pi} \frac{d\phi_S}{2\pi} \int_0^{2\pi} d\phi_h \sin(3\phi_h - \phi_S) \int_0^\infty d|\mathbf{P}_{h\perp}| |\mathbf{P}_{h\perp}| \frac{8J_3(|\mathbf{P}_{h\perp}||\mathbf{b}_T|)}{z^3 M^2 M_h |\mathbf{b}_T|^3} \left[ \frac{d\sigma}{dx_B dy d\phi_S dz_h d\phi_h |\mathbf{P}_{h\perp}| d|\mathbf{P}_{h\perp}|} \right] \\ &= \frac{\alpha^2}{yQ^2} \frac{y^2}{(1-\varepsilon)} \left( 1 + \frac{\gamma^2}{2x_B} \right) |\mathbf{S}_\perp| \varepsilon \sum_a e_a^2 \tilde{h}_{1T}^{\perp(2)a}(x, z^2 \mathbf{b}_T^2) \tilde{H}_1^{\perp(1)a}(z, \mathbf{b}_T^2) . \quad (22) \end{aligned}$$

The formalism in  $\mathbf{b}_T$ -space avoids convolutions, making it easier to perform a model independent analysis. The fundamental objects in this formalism are the (derivatives of) Fourier transformed TMDs  $\tilde{f}_1^{(0)}$ ,  $\tilde{g}_1^{(0)}$ ,  $\tilde{h}_1^{(0)}$ ,  $\tilde{f}_{1T}^{\perp(1)}$ ,  $\tilde{g}_{1T}^{\perp(1)}$ ,  $\tilde{h}_1^{\perp(1)}$ ,  $\tilde{h}_{1L}^{\perp(1)}$ ,  $\tilde{h}_{1T}^{\perp(2)}$  and fragmentation functions  $\tilde{D}_1^{(0)}$ ,  $\tilde{H}_1^{\perp(1)}$ . Theoretically, these  $|\mathbf{b}_T|$ -dependent distributions contain the same information as their conventional, momentum-dependent counterparts. In practice, however, only a limited range in  $|\mathbf{b}_T|$  is accessible with sufficient accuracy from experiments. Thus, to carry out the Fourier transformation back to conventional TMDs, model assumptions must be made in order to supplement information over the whole range of  $|\mathbf{b}_T|$ .

The  $|\mathbf{b}_T|$ -dependent distributions are also the objects that appear in the evolution equations that describe the scale dependence beyond tree level, see, e.g., Ref. [119].

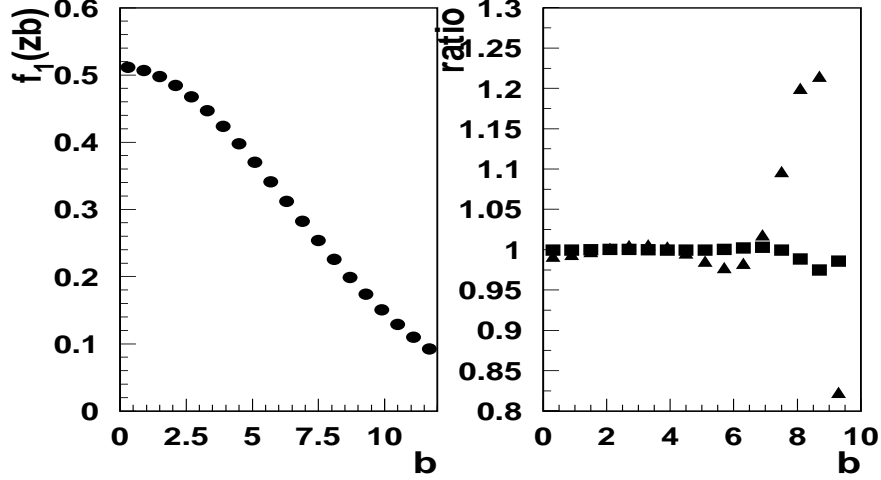


Figure 35: Extracted Fourier transformed  $f_1$  from unpolarized MC with Gaussian widths for  $f_1$  and  $D_1$  assumed as  $0.2 \text{ GeV}^2$  and  $0.25 \text{ GeV}^2$ , respectively, and average  $x$  and  $z$  at 0.2 and 0.5, respectively. The ratio is defined as the ratio of Fourier transformed  $b$ -dependences for integrals over  $k_T$  for  $P_T < P_{T_{max}}$  and the full  $P_T$ -integration. Squares and triangles correspond to  $P_{T_{max}} = 1.5$  and  $1.2 \text{ GeV}$ , respectively.

Lattice calculations of TMDs are performed in  $b$ -space rather than momentum space as well [49, 50]. This suggests that it is the  $|\mathbf{b}_T|$ -dependent quantities that are most suitable for a model independent analysis and comparison with lattice data.

The main questions to address when applying this procedure to CLAS12 data are the limited range in hadron transverse momenta and the low  $Q^2$ , as Fourier-transformed quantities receive (through the Fourier integral) contributions from the entire range of  $P_T$ , while the whole factorization formalism requires  $P_T \ll Q$ . The effect of the cut on the maximum value of  $P_T$  is shown in Fig. 35. Due to contributions to the cross section at high  $|\mathbf{P}_{h\perp}|$  that are not accounted for in the TMD factorized framework, further studies are needed as to whether and in what range of  $\mathbf{b}_T$  we can extract TMDs in Fourier space at JLab kinematics with moderate theoretical uncertainties. Most likely, precision measurements at large  $\mathbf{b}_T$  will require precision measurements at  $P_T$  in the range of 1.2-1.5 GeV, limiting the minimum  $Q^2$  to at least  $2 \text{ GeV}^2$ .

## 5 Summary and Beam Time Request

In this experiment we propose a study of the Transverse Momentum-Dependent (TMD) parton distributions via measurements of pion and kaon electro-production in SIDIS in the hard scattering regime ( $Q^2 > 1 \text{ GeV}^2$ ,  $W^2 > 4 \text{ GeV}^2$ ), using an 11 GeV electron beam from the upgraded CEBAF facility and the CLAS12 detector.

For this proposal, we request 100 days of beam time with high polarization of electrons at 11 GeV and a transversely polarized hydrogen target (80 days of data-taking plus 20 days for calibration, empty target runs and supportive tests). We expect to improve substantially the statistical precision of the HERMES measurements on the hydrogen target and the COMPASS measurements on the deuterium and proton targets, especially in the intermediate-to-large  $x$  region ( $x > 0.2$ ). The CLAS12 data covering large transverse momentum of pions will also be crucial in interpretation of the proposed Hall-A experiment on the  $^3\text{He}$  target.

The large acceptance of the CLAS12 detector permits a simultaneous scan of various variables ( $x_B$ ,  $z$ ,  $P_T$  and  $\phi$ ). Analysis of already existing electroproduction data from CLAS with unpolarized and longitudinally polarized targets has shown that the proposed measurements are feasible. Combined analysis of all three data sets will constrain different TMDs and relations between them, providing important input to global analysis of PDFs and will provide a substantial contribution to *nucleon tomography*.

### Beam Request

**We ask the PAC to award 100 days of beam time for a dedicated high statistics SIDIS experiment with the transversely polarized target.**

The measurement will produce precise data on the underlying quark transverse momentum distributions, providing important information on spin-orbit correlations. Understanding of spin-orbit correlations together with independent measurements related to spatial distributions and orbital angular momentum will help to construct a more complete picture of the nucleon in terms of elementary quarks and gluons going beyond the simple collinear partonic representation.

## References

- [1] J.P. Ralston and D.E. Soper, Nucl. Phys. B152 (1979) 109.
- [2] D.W. Sivers, Phys. Rev. D41 (1990) 83.
- [3] A. Kotzinian, Nucl. Phys. B441 (1995) 234, hep-ph/9412283.
- [4] P.J. Mulders and R.D. Tangerman, Nucl. Phys. B461 (1996) 197, hep-ph/9510301.
- [5] D. Boer and P.J. Mulders, Phys. Rev. D57 (1998) 5780, hep-ph/9711485.
- [6] P.J. Mulders and J. Rodrigues, Phys. Rev. D63 (2001) 094021, hep-ph/0009343.
- [7] A.V. Belitsky, X.d. Ji and F. Yuan, Phys. Rev. D69 (2004) 074014, hep-ph/0307383.
- [8] A. Bacchetta et al., JHEP 02 (2007) 093, hep-ph/0611265.
- [9] M. Burkardt, Phys. Rev. D62 (2000) 071503, hep-ph/0005108.
- [10] K. Goeke, M.V. Polyakov and M. Vanderhaeghen, Prog. Part. Nucl. Phys. 47 (2001) 401, hep-ph/0106012.
- [11] M. Burkardt, Int. J. Mod. Phys. A18 (2003) 173, hep-ph/0207047.
- [12] M. Diehl, Phys. Rept. 388 (2003) 41, hep-ph/0307382.
- [13] X. Ji, Ann. Rev. Nucl. Part. Sci. 54 (2004) 413.
- [14] A.V. Belitsky and A.V. Radyushkin, Phys. Rept. 418 (2005) 1, hep-ph/0504030.
- [15] S. Boffi and B. Pasquini, Riv. Nuovo Cim. 30 (2007) 387, 0711.2625.
- [16] X.d. Ji, Phys. Rev. Lett. 91 (2003) 062001, hep-ph/0304037.
- [17] S.J. Brodsky, D.S. Hwang and I. Schmidt, Phys. Lett. B530 (2002) 99, hep-ph/0201296.
- [18] J.C. Collins, Phys. Lett. B536 (2002) 43, hep-ph/0204004.
- [19] X. Ji and F. Yuan, Phys. Lett. B543 (2002) 66, hep-ph/0206057.
- [20] A.V. Belitsky, X. Ji and F. Yuan, Nucl. Phys. B656 (2003) 165, hep-ph/0208038.
- [21] D. Boer, S.J. Brodsky and D.S. Hwang, Phys. Rev. D67 (2003) 054003, hep-ph/0211110.



- [22] D. Boer, P.J. Mulders and F. Pijlman, Nucl. Phys. B667 (2003) 201, hep-ph/0303034.
- [23] X. Ji, J. Ma and F. Yuan, Phys. Rev. D71 (2005) 034005, hep-ph/0404183.
- [24] J.C. Collins and A. Metz, Phys. Rev. Lett. 93 (2004) 252001, hep-ph/0408249.
- [25] K. Goeke, A. Metz and M. Schlegel, Phys. Lett. B618 (2005) 90, hep-ph/0504130.
- [26] S. Meissner, A. Metz and K. Goeke, Phys. Rev. D76 (2007) 034002, hep-ph/0703176.
- [27] C. Lorce and B. Pasquini, (2011), 1104.5651.
- [28] S.J. Brodsky, D.S. Hwang and I. Schmidt, Nucl. Phys. B642 (2002) 344, hep-ph/0206259.
- [29] Z.B. Kang and J.W. Qiu, Phys. Rev. Lett. 103 (2009) 172001, 0903.3629.
- [30] M. Anselmino et al., Phys. Rev. D71 (2005) 074006, hep-ph/0501196.
- [31] J.C. Collins et al., Phys. Rev. D73 (2006) 094023, hep-ph/0511272.
- [32] W. Vogelsang and F. Yuan, Phys. Rev. D72 (2005) 054028, hep-ph/0507266.
- [33] M. Anselmino et al., hep-ph/0805.2677 (2008), 0805.2677.
- [34] HERMES, A. Airapetian et al., Phys. Rev. Lett. 103 (2009) 152002, 0906.3918.
- [35] The COMPASS, M.G. Alekseev et al., Phys. Lett. B692 (2010) 240, 1005.5609.
- [36] I.O. Cherednikov and N.G. Stefanis, Phys. Rev. D77 (2008) 094001, 0710.1955.
- [37] I.O. Cherednikov and N.G. Stefanis, Nucl. Phys. B802 (2008) 146, 0802.2821.
- [38] I.O. Cherednikov and N.G. Stefanis, Phys. Rev. D80 (2009) 054008, 0904.2727.
- [39] Fermilab E906/SeaQuest, P. Reimer et al., (2001), Fermilab Proposal 906, Unpublished, <http://projects-docdb.fnal.gov/cgi-bin/RetrieveFile?docid=402>.
- [40] E906/SeaQuest, P. Reimer et al., (2006), Experiment update to Fermilab PAC <http://projects-docdb.fnal.gov/cgi-bin/ShowDocument?docid=395>.
- [41] L.B. et al., (2011), [http://www.bnl.gov/npp/docs/pac0611/DY\\_pro\\_110516\\_final.2.pdf](http://www.bnl.gov/npp/docs/pac0611/DY_pro_110516_final.2.pdf).
- [42] D. Boer, (2011), 1105.2543.
- [43] H. Mkrtchyan et al., Phys. Lett. B665 (2008) 20, 0709.3020.

- [44] The CLAS, H. Avakian et al., Phys. Rev. Lett. 105 (2010) 262002, 1003.4549.
- [45] Z. Lu and B.Q. Ma, Nucl. Phys. A741 (2004) 200, hep-ph/0406171.
- [46] M. Anselmino et al., Phys. Rev. D74 (2006) 074015, hep-ph/0608048.
- [47] B. Pasquini, S. Cazzaniga and S. Boffi, Phys. Rev. D78 (2008) 034025, 0806.2298.
- [48] C. Bourrely, F. Buccella and J. Soffer, (2010), 1008.5322.
- [49] P. Hagler et al., Europhys. Lett. 88 (2009) 61001, 0908.1283.
- [50] B.U. Musch et al., (2010), 1011.1213.
- [51] Z.B. Kang et al., Phys. Rev. D83 (2011) 094001, 1103.1591.
- [52] J. She, J. Zhu and B.Q. Ma, Phys. Rev. D79 (2009) 054008, 0902.3718.
- [53] H. Avakian et al., (2008), 0805.3355.
- [54] H. Avakian et al., Phys. Rev. D81 (2010) 074035, 1001.5467.
- [55] H. Avakian et al., Mod. Phys. Lett. A24 (2009) 2995, 0910.3181.
- [56] M. Burkardt and H. BC, Phys. Rev. D79 (2009) 071501, 0812.1605.
- [57] X.D. Ji, Phys. Rev. Lett. 78 (1997) 610, hep-ph/9603249.
- [58] P. Schweitzer, T. Teckentrup and A. Metz, Phys. Rev. D81 (2010) 094019, 1003.2190.
- [59] S. Boffi et al., Phys. Rev. D79 (2009) 094012, 0903.1271.
- [60] B. Pasquini and F. Yuan, Phys. Rev. D81 (2010) 114013, 1001.5398.
- [61] B.U. Musch, (2009), 0907.2381.
- [62] J.C. Collins, Nucl. Phys. B396 (1993) 161, hep-ph/9208213.
- [63] COMPASS, A. Kotzinian, (2007), arXiv:0705.2402 [hep-ex].
- [64] COMPASS, P. Abbon et al., Nucl. Instrum. Meth. A577 (2007) 455, hep-ex/0703049.
- [65] HERMES, A. Airapetian et al., Phys. Rev. Lett. 84 (2000) 4047, hep-ex/9910062.
- [66] HERMES, A. Airapetian et al., Phys. Rev. Lett. 94 (2005) 012002, hep-ex/0408013.

- [67] COMPASS, V.Y. Alexakhin et al., Phys. Rev. Lett. 94 (2005) 202002, hep-ex/0503002.
- [68] COMPASS, E.S. Ageev et al., Nucl. Phys. B765 (2007) 31, hep-ex/0610068.
- [69] R.L. Jaffe and X.D. Ji, Nucl. Phys. B375 (1992) 527.
- [70] D.W. Sivers, Phys. Rev. D43 (1991) 261.
- [71] M. Anselmino and F. Murgia, Phys. Lett. B442 (1998) 470, hep-ph/9808426.
- [72] X.d. Ji, J.P. Ma and F. Yuan, Phys. Lett. B597 (2004) 299, hep-ph/0405085.
- [73] X. Ji et al., Phys. Rev. D73 (2006) 094017, hep-ph/0604023.
- [74] J.w. Qiu and G.F. Sterman, Phys. Rev. Lett. 67 (1991) 2264.
- [75] E581, D.L. Adams et al., Z. Phys. C56 (1992) 181.
- [76] STAR, J. Adams et al., Phys. Rev. Lett. 92 (2004) 171801, hep-ex/0310058.
- [77] G.A. Miller, Phys. Rev. C76 (2007) 065209, 0708.2297.
- [78] M. Burkardt, hep-ph 0709.2966 (2007), 0709.2966.
- [79] A.M. Kotzinian and P.J. Mulders, Phys. Rev. D54 (1996) 1229, hep-ph/9511420.
- [80] E. Leader, A.V. Sidorov and D.B. Stamenov, Phys. Lett. B462 (1999) 189, hep-ph/9905512.
- [81] H.C. Kim, M.V. Polyakov and K. Goeke, Phys. Lett. B387 (1996) 577, hep-ph/9604442.
- [82] HERMES, A. Airapetian et al., Phys. Lett. B693 (2010) 11, 1006.4221.
- [83] M.G. Alekseev et al., Eur. Phys. J. C70 (2010) 39, 1007.1562.
- [84] M. Anselmino et al., Nucl. Phys. Proc. Suppl. 191 (2009) 98, 0812.4366.
- [85] A. Bacchetta et al., Phys. Rev. D65 (2002) 094021, hep-ph/0201091.
- [86] A.V. Efremov, K. Goeke and P. Schweitzer, Phys. Rev. D67 (2003) 114014, hep-ph/0208124.
- [87] A.M. Kotzinian et al., (1999), hep-ph/9908466.
- [88] BELLE, K. Abe et al., Phys. Rev. Lett. 96 (2006) 232002, hep-ex/0507063.

- [89] Belle, A. Ogawa et al., AIP Conf. Proc. 915 (2007) 575.
- [90] Belle, R. Seidl et al., Phys. Rev. D78 (2008) 032011, 0805.2975.
- [91] M. Anselmino et al., (2007), hep-ph/0701006.
- [92] COMPASS, B. Parsamyan, Eur. Phys. J. ST 162 (2008) 89, 0709.3440.
- [93] H. Avakian et al., Phys. Rev. Lett. 99 (2007) 082001, 0705.1553.
- [94] A. Kotzinian, B. Parsamyan and A. Prokudin, Phys. Rev. D73 (2006) 114017, hep-ph/0603194.
- [95] R.L. Jaffe, Int. J. Mod. Phys. A18 (2003) 1141, hep-ph/0201068.
- [96] J. Zhu and B.Q. Ma, (2011), 1104.5545.
- [97] BRAHMS, I. Arsene et al., Phys. Rev. Lett. 101 (2008) 042001, 0801.1078.
- [98] BRAHMS, J. Lee et al.
- [99] C.S. for COMPASS, (2011), DIS 2011 Conference.
- [100] G. F. and L. R., J. Phys. Conf. Ser. 295 (2011) 012092, 1011.5422.
- [101] BELLE Collaboration, R. Seidl et al., Phys.Rev. D78 (2008) 032011.
- [102] HERMES, G. F. and L. R., AIP Conf. Proc. 1149 (2009) 423, 0901.2438.
- [103] G.S.f.t.C. Collaboration, (2010), 1012.4910.
- [104] I.G. for BaBar.
- [105] H. Avakian et al., JLab Experiment E12-07-015 (2008).
- [106] A. Bacchetta et al., Phys. Lett. B659 (2008) 234, 0707.3372.
- [107] HERMES, A. Airapetian et al., Phys. Lett. B562 (2003) 182, hep-ex/0212039.
- [108] J.C. Collins et al., Phys. Rev. D73 (2006) 014021, hep-ph/0509076.
- [109] European Muon, M. Arneodo et al., Z. Phys. C34 (1987) 277.
- [110] G. Cates et al., JLab Experiment E12-11-007 (2008).
- [111] H. Hao, Q. X. and P. J.-C., JLab Experiment E12-11-007 (2008).
- [112] H. Gao et al., Eur. Phys. J. Plus 126 (2011) 2, 1009.3803.
- [113] E143, K. Abe et al., Phys. Rev. D58 (1998) 112003, hep-ph/9802357.

- [114] CLAS, . A.Sandorfi et al., CLAS proposal E06-101 (2006).
- [115] A. Caracappa and C. Thorn, AIP Conf. Proc. 675 (2003) 867.
- [116] C. Thorn and . Caracappa, AIP Conf. Proc. (2007) (in press).
- [117] Jefferson Lab Hall A, M.K. Jones et al., Phys. Rev. Lett. 84 (2000) 1398, nucl-ex/9910005.
- [118] D. Boer et al., (2011), in preparation.
- [119] A. Idilbi et al., Phys. Rev. D70 (2004) 074021, hep-ph/0406302.